



Research paper

Improving potency and metabolic stability by introducing an alkenyl linker to pyridine-based histone deacetylase inhibitors for orally available RUNX3 modulators



Doona Song^a, Chulho Lee^a, Yoon Jeong Kook^{a, c}, Soo Jin Oh^b, Jong Soon Kang^b, Hyun-Jung Kim^a, Gyoonhee Han^{a, c, *}

^a Translational Research Center for Protein Function Control, Department of Biotechnology, Yonsei University, Seoul 120-749, Republic of Korea

^b Bioevaluation Center, Korea Research Institute of Bioscience and Biotechnology, Ochang, Cheongwon, Chungbuk 363-883, Republic of Korea

^c Department of Integrated OMICS for Biomedical Sciences (WCU Program), Yonsei University, Seoul 120-749, Republic of Korea

ARTICLE INFO

Article history:

Received 24 June 2016

Received in revised form

10 November 2016

Accepted 29 November 2016

Available online 1 December 2016

Keywords:

RUNX3

RUNX3 acetylation

HDAC inhibition

Epigenetic control

Protein stabilization

ABSTRACT

RUNX3, a tumor suppressor, is suppressed in various cancers by abnormal epigenetic changes. Histone deacetylases (HDACs) can deacetylate the lysine residues of RUNX3, followed by degradation via a ubiquitin-mediated pathway. Inhibition of HDAC leads to functional restoration of the RUNX3 protein by epigenetic expression and RUNX3 protein stabilization. We previously reported a series of HDAC inhibitors that restored RUNX3 function. In the present study, we introduced an alkenyl linker group to pyridine-based HDAC inhibitors to improve their potencies and chemical properties. This alkenyl linker made the compounds more rigid, facilitating a better fit than alkyl moieties to the active site of HDAC proteins. Most compounds in this series exhibited potent RUNX3 activities, HDAC inhibitory activities, and inhibitory activities towards the growth of human cancer cell lines. Notably, one of these derivatives, (*E*)-3-(1-cinnamyl-2-oxo-1,2-dihydropyridin-3-yl)-*N*-hydroxyacrylamide (**7k**), showed excellent properties in a microsomal stability study, in a xenograft study, and in an *in vivo* pharmacokinetic evaluation. Modulation of RUNX3 therefore results in highly potent and orally available anticancer chemotherapeutic agents.

© 2016 Elsevier Masson SAS. All rights reserved.

1. Introduction

Epigenetics is currently defined as an inheritable change without DNA sequence modifications [1]. Disorders in such changes affect a wide variety of pathologies including cancers [2,3]. There are two major mechanisms of epigenetic regulations involving DNA methylation and covalent histone modification. Histones can undergo multiple posttranslational modifications by diverse enzymes such as histone acetyltransferases (HATs), histone deacetylases (HDACs), histone methyltransferases (HMTs), and histone demethylases (HDMs) [4]. HATs and HDACs exert their functions within complexes that include multiple HATs, HDACs, transcription coactivators, and corepressors [5]. HDAC activities are modulated in

many ways involving protein-protein interactions, post-translational modifications, subcellular localization, and the availability of metabolic cofactors [6]. Although the relationships between aberrant expression of various HDACs and cancer remain largely correlative, the altered expression of HDACs can play an important role in tumor onset and progression, so HDACs are attractive targets for the development of therapeutic agents [7]. Regarding acetylation of multiple HDAC substrates, a single pathway or multiple pathways may be involved in HDAC inhibitor (HDACi)-induced cell death. HDACi can be classified into several structural classes including hydroxamates, cyclic peptides, aliphatic acids, and benzamides [6]. Trichostatin A (TSA, Fig. 1) was the first natural product isolated and shown to inhibit HDACs [8]. SAHA, a structurally close analogue to TSA, was the first HDACi to be approved for clinical use by the Food and Drug Administration (Fig. 1) [9]. A series of hydroxamic acids has been shown to block HDACs and affect cell proliferation at nanomolar concentrations [10]. Despite the outstanding efficacy of HDACs, they have major disadvantages such as nonspecificity and resistance, which are

* Corresponding author. Translational Research Center for Protein Function Control, Department of Biotechnology, Yonsei University, Seoul 120-749, Republic of Korea.

E-mail address: gyoonhee@yonsei.ac.kr (G. Han).

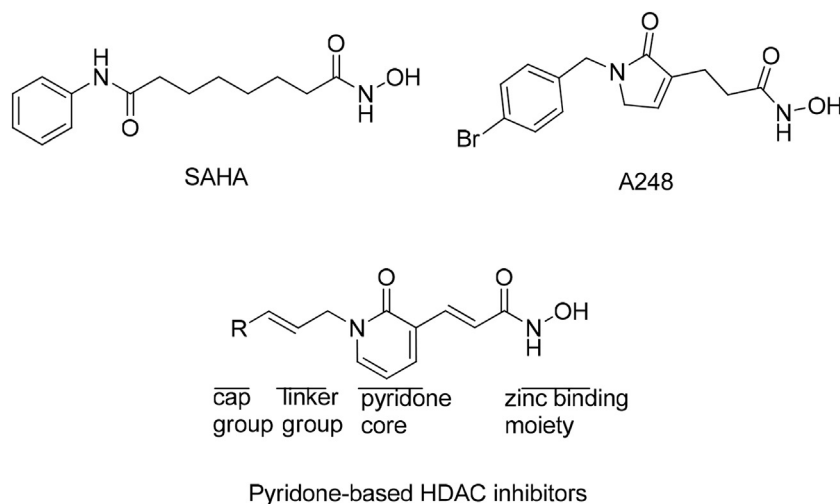


Fig. 1. Chemical structures of hydroxamic acid-based deacetylase inhibitors. A248 was reported in previous study [29].

common disadvantages in epigenetic therapies [11–13]. A new approach is therefore needed to eliminate these disadvantages.

Epigenetic alteration can lead to a variety of transcriptional effects involving the imbalance between HDACs and HATs. Tumor suppressors, such as RUNX3, are suppressed in various cancers by abnormal epigenetic changes [14,15]. All RUNX family members share the central Runt domain, which is a well-conserved domain that recognizes specific DNA sequences. RUNX1 and RUNX2 are involved in hematopoiesis and osteogenesis, respectively, and are genetically altered in leukemia and bone disease [16]. In contrast, RUNX3 is required for the control of cell proliferation of the gastric epithelium, neurogenesis of the dorsal root ganglia, and differentiation of T-cells [17]. RUNX3 interacts with p300 HAT and is acetylated at lysine residues, which is necessary for its transcriptional activity. This acetylation is reversed by HDACs that are in competition with Smurf1-mediated ubiquitination [18]. HDACs cause the deacetylation of RUNX3, followed by degradation by the ubiquitin-mediated pathway. HDAC inhibitors therefore increase the acetylation of RUNX3, and improve the stability and transcriptional activity of RUNX3 [19]. RUNX3 inactivation is usually caused by epigenetic changes, rather than rare mutations [15]. RUNX3 may therefore be an excellent target for anti-cancer therapy because it functions as a tumor suppressor and can be recovered by RUNX3-targeted agents [20].

In a previous study, we reported that the restoration and stabilization of RUNX3 levels by HDAC inhibition could be a new approach in cancer treatment [21]. Furthermore, a series of HDAC inhibitors introduced a pyridone core and an olefin moiety to improve chemical and metabolic stabilities [22]. It is probable that the olefin moiety of HDAC inhibitors is important for activity. In the present study, we designed a new series of pyridone-based HDAC inhibitors that contained an alkenyl group as a linker group to improve the potencies and efficacies as an anticancer agent. A total of 22 compounds were synthesized and tested using various biological assays. We conducted *in vitro* biological evaluations including evaluations of RUNX transcriptional activation levels and HDAC inhibitory activities, plus cancer cell growth inhibitory activities. The synthesized compounds were tested for their effects on the posttranslational acetylation of RUNX3 involving protein stabilization through epigenetic regulation, and were tested for microsomal stability to monitor their physicochemical properties. Furthermore, *in vivo* xenograft studies and pharmacokinetic profiles were performed using the screened compounds to identify orally available candidates. The high potency, stability, and *in vivo*

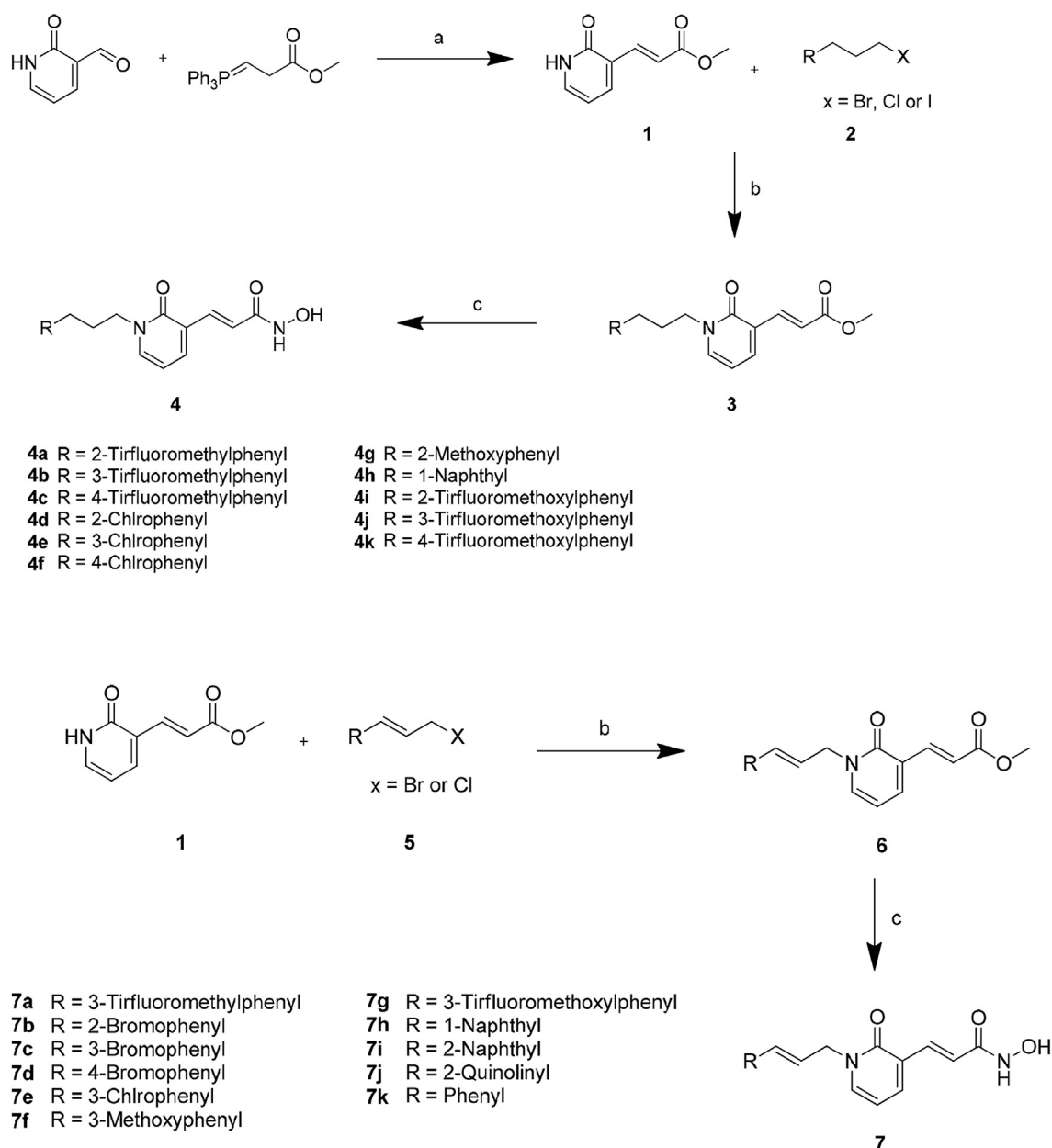
efficacy of synthesized compounds suggested that the RUNX3 modulators can be used for cancer therapy.

2. Results, methods, and discussion

2.1. Strategies and chemistry

In a previous study, the pyridone core HDAC inhibitors with a hydroxamate conjugated system were reported to improve the chemical and metabolic stabilities of hydroxamic acid [22]. A three-dimensional quantitative structure-activity relationship (3D QSAR) and docking simulation study indicated that hydroxamic acid chelated to zinc ion in the HDAC active site passes through a narrow hydrophobic tunnel, and that the bulky aromatic cap groups are important for inhibitory activity [23]. Based on these studies, we synthesized potent and orally available RUNX3 modulators based on HDAC inhibitors (Fig. 1). We designed and synthesized a new scaffold composed of an alkenyl group on the three carbon linker group between the cap group and the pyridone core. This olefin moiety made the compounds more rigid and more stable than the alkyl moiety. Moreover, this rigidity facilitated a better fit to the HDAC active site, and the increased chemical stability protected the compounds from enzymatic hydrolysis to improve their activities and physicochemical properties as RUNX3 modulators. These compounds also contained diverse functional phenyl, bromophenyl, chlorophenyl, methoxyphenyl, naphthyl, trifluoromethylphenyl, and trifluoromethoxyphenyl groups as the cap groups that were evaluated in structure-activity relationship studies (SARs).

The general procedures for the synthesis of pyridone-based RUNX3 modulators are outlined in Scheme 1. Based on the previous SAR study, more alkyl linker and new alkenyl linker derivatives were designed and synthesized [22]. Scheme 1 shows the procedure for the olefin linker (between the cap group and the pyridone core) in the pyridone-based derivatives that were used to produce a new series of RUNX3 modulators. Commercially available carbaldehyde and Wittig reagent were refluxed in dichloromethane to produce the Wittig products, **1**. Compounds **3** and **6** were produced by an N-alkylation reaction of compound **1** [(*E*)-methyl 3-(2-oxo-1,2-dihydropyridin-3-yl) acrylate] with synthetic or commercial aromatic alkyl halides **2** and **5**, respectively. The hydroxamic acid analogues, **4** and **7**, were obtained by reacting the esters of the pyridones with KONH_2 (1.7 M in MeOH) in MeOH at low temperature.



Scheme 1. General procedure for synthesis of pyridone core-based deacetylase inhibitors with an alkyl linker moiety (**4**) or conjugated linker moiety (**7**). Reagents: (a) CH_2Cl_2 , reflux; (b) K_2CO_3 , acetone, reflux; (c) KONH_2 (1.7 M in MeOH), MeOH, 0°C .

2.2. *In vitro* biological evaluation

All synthesized compounds (**4a–4k** and **7a–7k**) were tested for *in vitro* HDAC inhibitory activities involving RUNX transcriptional and cancer cell growth inhibitory activities. The results are summarized in Table 1, using SAHA as a positive control.

Inhibition of HDAC activity by all of the synthesized compounds was monitored by the HDAC fluorescent activity assay kit using whole HDACs from HeLa cell extracts. While HDAC inhibitory activities of alkyl linker compounds varied from 0.07 to 0.48 μM , those of alkenyl-linker analogues varied from 0.001 to 0.1 μM . All alkenyl linker analogues exhibited better HDAC inhibitory activities than SAHA, with an IC_{50} of 0.11 μM . RUNX transcriptional activities of the synthesized compounds were monitored using the luciferase assay system and expressed as the percentage of activation compared to a positive control, fibroblast growth factor 2 (FGF-2), a

known upregulator of RUNX2 expression. This assay system was useful for estimating the transcriptional activity of RUNX3, because all three RUNX proteins shared the same consensus sequences in the promoter regions of the target genes [24]. A total of 29 compounds were evaluated, showing 40–470% of the relative RUNX3 transcriptional activity compared to FGF-2 (Table 1). They were classified into three groups based on these results, except for compounds with RUNX activation <100%. Remarkably, most olefin linker analogues were excellent activators of RUNX3 transcription except **7d** (R = 4-bromophenyl). Among the alkyl linker derivatives, compound **4c** (R = 4-trifluoromethylphenyl), **4f** (R = 4-chlorophenyl), and **4k** (R = 4-trifluoromethoxyphenyl) showed much lower activities than FGF-2. All alkenyl linker analogues showed better RUNX transcription activities than SAHA, which showed a moderate RUNX activity of 80.2%. Compared to alkyl linker compounds, alkenyl linker analogues exhibited high average

Table 1
Percentage of RUNX transcriptional activation relative to fibroblast growth factor (FGF)-2, inhibition of deacetylase enzyme activity and cancer cell growth by pyridone-based analogues.

Compd	linker	R	Activation (%)	Group	IC ₅₀ (μM)		GI ₅₀ (μM)				
			RUNX		HDAC	PC-3	MDA-MB-231	ACHN	HCT-15	NCI-H23	NUGC-3
4a	alkyl	2-Trifluoromethylphenyl	105.6	III	0.11	1.29	1.35	0.95	0.88	1.14	0.99
4b	alkyl	3-Trifluoromethylphenyl	118.5	III	0.13	1.14	1.69	0.85	0.72	0.98	0.83
4c	alkyl	4-Trifluoromethylphenyl	39.4	–	0.37	1.98	3.94	2.32	1.01	3.22	2.36
4d	alkyl	2-Chlorophenyl	127.4	III	0.08	0.76	0.55	0.58	1.35	0.50	0.31
4e	alkyl	3-Chlorophenyl	129.0	III	0.07	0.83	0.41	0.63	1.19	0.48	0.71
4f	alkyl	4-Chlorophenyl	53.1	–	0.14	1.41	1.10	1.48	1.96	1.33	1.57
4g	alkyl	2-Methoxyphenyl	152.4	II	0.08	0.86	0.64	0.48	0.47	0.68	0.29
4h	alkyl	1-Naphthyl	225.2	I	0.03	0.06	0.08	0.02	0.11	0.07	0.03
4i	alkyl	2-Trifluoromethoxyphenyl	88.7	–	0.09	0.22	0.30	0.27	0.53	0.33	0.14
4j	alkyl	3-Trifluoromethoxyphenyl	72.6	–	0.12	0.41	0.58	0.52	0.89	0.64	0.41
4k	alkyl	4-Trifluoromethoxyphenyl	31.2	–	0.28	0.56	1.37	1.49	1.10	1.63	0.96
4l^a	alkyl	2-Bromophenyl	162.8	II	0.48	1.86	2.89	1.92	1.58	1.88	1.50
4m^a	alkyl	3-Bromophenyl	100.8	III	0.10	1.26	1.85	0.74	1.16	1.22	1.20
4n^a	alkyl	4-Bromophenyl	53.8	–	0.21	3.97	4.38	4.19	7.45	4.88	4.02
4o^a	alkyl	3-Methoxyphenyl	142.1	III	0.03	0.70	0.72	0.76	1.59	0.87	1.05
4p^a	alkyl	4-Methoxyphenyl	97.6	–	0.14	1.78	1.36	0.98	0.90	1.31	0.97
4q^b	alkyl	2-Naphthyl	131.9	III	0.07	0.35	0.31	0.19	0.38	0.29	0.14
4r^b	alkyl	Phenyl	81.8	–	0.34	3.93	3.53	3.84	2.82	3.80	2.59
7a	olefin	3-Trifluoromethylphenyl	183.0	II	0.03	0.28	0.38	0.28	0.72	0.31	0.29
7b	olefin	2-Bromophenyl	180.2	II	0.07	0.05	0.19	0.05	0.31	0.10	0.19
7c	olefin	3-Bromophenyl	164.8	II	0.07	0.36	0.52	0.11	0.36	0.49	0.26
7d	olefin	4-Bromophenyl	89.2	–	0.08	0.57	0.81	0.40	0.63	0.76	0.56
7e	olefin	3-Chlorophenyl	247.6	I	0.02	0.13	0.14	0.17	0.68	0.28	0.21
7f	olefin	3-Methoxyphenyl	331.1	I	0.03	0.39	0.57	0.38	0.49	0.15	0.32
7g	olefin	3-Trifluoromethoxyphenyl	148.1	III	0.04	0.57	0.61	0.56	0.63	0.24	0.56
7h	olefin	1-Naphthyl	461.8	I	0.001	0.03	0.07	0.03	0.03	0.03	0.07
7i	olefin	2-Naphthyl	230.7	I	0.02	0.28	0.20	0.14	0.25	0.03	0.16
7j	olefin	2-Quinolinylnyl	324.9	I	0.04	0.23	0.16	0.23	0.89	0.23	0.11
7k	olefin	Phenyl	111.0	III	0.09	0.47	0.73	0.69	1.16	1.11	0.35
SAHA			80.2		0.11	2.69	2.00	4.22	2.49	2.34	2.94
A248			102.6		0.11	2.94	0.60	0.41	1.65	3.46	ND ^c
Average value of olefin linker analogues			224.76		0.04	0.31	0.40	0.27	0.56	0.34	0.28
Average value of alkyl linker analogues			110.63		0.16	1.24	1.45	1.20	1.44	1.36	1.08
Average value on HDAC inhibition of group I			0.02								
Average value on HDAC inhibition of group II			0.15								
Average value on HDAC inhibition of group III			0.08								

^a Compounds were reported in our previous work [30].

^b Compounds reported in our previous work [22].

^c No Data.

values of RUNX3 transcriptional activation (Table 1). Compounds **4h**, **7h**, **7i**, and **7j**, which had a simple polycyclic group in common on the cap moiety, strongly activated the RUNX3 transcription at 225.2%, 461.8%, 230.7%, and 324.9%, respectively. All synthesized compounds were classified into three groups based on their HDAC inhibitory activities and RUNX activation levels [21]. For RUNX activation, seven compounds in group I showed strong RUNX transcriptional activation > 200%. For group II, the compounds showed RUNX transcriptional activation levels between 150 and 200%. For group III, the compounds showed RUNX transcriptional activation levels between 100 and 150%. The HDAC inhibitory activities showed a similar tendency, based upon the group involved in RUNX activation. The averages for each group, were Group I, 0.02 μM; Group II, 0.15 μM; and Group III, 0.08 μM (Table 1).

It was possible that the potency of HDAC inhibition was correlated with the potency of RUNX activation. Inhibition of cancer cell growth of the prepared analogues was therefore evaluated using the sulforhodamine B (SRB) assay that showed GI₅₀ values using PC-3 (prostate), MDA-MB-231 (breast), ACHN (renal), HCT-15 (colon), NCI-H23 (non-small cell lung), and NUGC-3 (gastric) cancer cell lines. As shown in Table 1, most compounds were more active than SAHA in the six cancer cell lines, and were the most potent against the NUGC-3 cell line. Based upon the average of GI₅₀ values, almost all alkenyl linker compounds showed better

antiproliferative activities than the alkyl linker analogues.

Taken together, the results from *in vitro* assays (RUNX transcriptional activation, HDAC inhibitory activity, and cancer cell growth inhibitory activity) showed that the synthesized compounds with alkenyl-linker moieties were more potent than those with alkyl linker moieties.

2.3. SAR

To identify even more effective compounds, a SAR study was conducted based on *in vitro* activities of the functional groups, the cap groups, and the various linker group modifications between the pyridone-based core and the cap group. The various cap group substituents involved halogenphenyl, trifluoromethylphenyl, trifluoromethoxyphenyl, methoxyphenyl, naphthyl, and quinolinylnyl groups. Overall, compounds with naphthyl, quinolinylnyl, methoxyphenyl, and chlorophenyl substituents as the cap group showed the best HDAC inhibitory activities, RUNX transcriptional activities, and cell growth inhibitory activities. In addition, all compounds with a simple polycyclic group on the cap moiety (**4h**, **7h**, **7i**, and **7j**) strongly induced RUNX transcription > 200% (**4h** = 225.2%, **7h** = 461.8%, **7i** = 230.7%, and **7j** = 324.9%) and inhibited the HDAC activity with an IC₅₀ < 0.04 μM (**4h** = 0.03 μM, **7h** = 0.001 μM, **7i** = 0.02 μM, and **7j** = 0.04 μM). Compared to alkyl linker

compounds, the alkenyl linker analogues exhibited a higher average value of RUNX transcriptional activation.

To evaluate the effect on the position of the substituent phenyl group, the substituents were introduced to the ortho, meta, or para positions. For the CF₃ group in the cap group, the relative RUNX transcriptional and HDAC inhibitory activities showed activities of 105.6%/0.11 μM (**4a**, ortho position), 118.5%/0.13 μM (**4b**, meta position), and 39.4%/0.37 μM (**4c**, para position). In a similar manner, the RUNX activation and HDAC inhibitory activities showed similar tendencies in analogues with chlorophenyl (**4d–4f**), trifluoromethoxyphenyl (**4i–4k**), and methoxyphenyl (**4g**, **4o**, and **4p**) substituents. Most compounds which had ortho- and meta-substituted analogues therefore showed better activities of HDAC inhibition, RUNX activation, and cell growth inhibitory activities than para-substituted analogues.

In a previous study, the introduction of an olefin system between the pyridone core and hydroxamate group was crucial for optimizing biological potency and improving pharmacokinetic properties. In the present study, the effects of the alkenyl system between the cap and core structures were examined. Alkenyl groups made the compounds more rigid and more stable than alkyl moieties (Fig. S1, Table S1). This rigidity could lead to a better fit to the HDAC active site, and the chemical stability could protect the compounds from enzymatic hydrolysis. Furthermore, the introduction of a double bond on the linker moiety enhanced the potency as an RUNX3 modulator (Table 1).

All compounds showed excellent HDAC inhibitory activities with IC₅₀ values < 0.1 μM and RUNX activation values > 100%, except **7d** (4-bromophenyl). Most of the synthesized compounds with an alkenyl linker had improved HDAC inhibition, RUNX3 activation, and cancer cell inhibition. Most notably, compound **7k** increased the IC₅₀ (0.09 μM), GI₅₀ (0.34–1.10 μM), and RUNX activation (111.0%) compared to compound **4r** (0.34 μM, 2.58–3.92 μM, and 81.8%, respectively). The average RUNX activation and HDAC inhibition changed from 103.92%/0.14 μM (alkyl linker) to 229.33%/0.04 μM (alkenyl linker). The growth inhibition of cancer cells was also improved. The GI₅₀ values were decreased more than half for most of the cancer cell lines. In addition, the alkenyl and alkyl linker analogues with the same R groups could be directly compared. Based on various *in vitro* assays, the introduction of an alkenyl group on the linker moiety therefore resulted in the best activity.

2.4. RUNX3 stabilization

Acetylation of RUNX3 was recently reported to be essential for the retention of RUNX3 stability [19]. To examine the stabilization of RUNX3, we evaluated the acetylation level of RUNX3 after treating cells with 13 compounds (**4d–4h**, **7a**, **7c**, and **7e–7k**) by comparing them with SAHA as a positive control that had HDAC inhibition and RUNX3 transcriptional activation activities of <0.1 μM and >100%, respectively. In parallel, we characterized the expression of RUNX3 and the acetylation of histone (H3), to determine if these compounds were nonspecific epigenetic activators. Acetylation of H3 resulted in HDAC inhibition and hyperacetylation of H3 that led to upregulation of nonspecific gene expression. The ratio of Ac-RUNX3 to Ac-histone (H3) was also estimated to determine the specificity of the compounds for RUNX3 stabilization over nonspecific gene expression. All selected analogues showed higher ratios of acetylated RUNX3/acetylated H3 than SAHA (Fig. 2C). Most notably, alkyl derivatives **4d**, **4g**, and **4h** showed 4–6 fold more acetylated RUNX protein than SAHA. Most alkenyl derivatives showed 2–4 fold greater RUNX3 acetylation levels compared with that of SAHA. With a low ratio of Ac-RUNX3/Ac-histone < 1, all compounds (**7a**, **7e**, **7f**, **7h**, and **7g**) showed strong inhibition of HDAC (IC₅₀ < 0.04 μM) and RUNX3 (over 150%) except

compound **7g** (148.1%, also a strong RUNX activity). Based on these results, the compounds with high HDAC inhibitory activity tended to show nonspecific activity because of strong epigenetic and transcriptional activations. Among the alkenyl compounds, **7i** and **7k** showed the best ratio of Ac-RUNX3/para position-Ac-histone of 4.3 and 3.8, respectively.

2.5. Microsomal stability

Based on results of *in vitro* assays, the alkenyl analogues were potential RUNX modulators. The metabolic stability profiles were then determined to identify the effects of the olefin group between the cap group and the core on ADME (Absorption, Distribution, Metabolism, and Excretion) properties. Metabolic stability profiles of five olefin-linker analogues (**7b**, **7c**, **7i**, **7j**, and **7k**) that exhibited Ac-RUNX3/Ac-H3 ratios > 1 were evaluated in mouse liver microsomes (Table 2). During oxidative conditions using mouse liver microsomes involved in NADPH-dependent cytochrome P450 (CYP450)-mediated oxidative reactions, most olefin linker analogues showed increases of metabolic stability > 10–20% compared with those of their corresponding alkyl linker compounds, except **7i** (Table 2). For example, compounds **4o**, **7c**, **7j**, and **7k** showed high microsomal stability (65.1%, 40.9%, 65.8%, and 88.2%, respectively, remaining after 30 min), and compounds **4n**, **7b** and **7i** also showed moderate metabolic stability (35.5%, 33.6%, and 27.9%, respectively, remaining after 30 min). Taken together, the alkenyl-linker analogues showed higher stability than the alkyl-linker analogues against enzymatic hydrolysis.

2.6. In vivo antitumor activity

To determine the pharmacological efficacy of the selected RUNX3 modulators, we tested these compounds in an *in vivo* xenograft model. Based on *in vitro* biological evaluations and evaluations of microsomal stability, the alkenyl linker analogues were more potent than the alkyl linker analogues, so three compounds (**7c**, **7j**, and **7k**) were selected for further evaluation. These compounds had relatively better cancer cell growth inhibition activities in gastric cancer cell lines, so the MKN28 cell line was selected as a xenograft model, which is the same type of gastric cancer cell without expression of RUNX3 because of epigenetic inactivation by DNA methylation [25]. Reactivation of RUNX3 by AZA and TSA in MKN28 cells has been previously reported [15], so this *in vivo* MKN28 xenograft regression model monitored the effects of the compounds involving reactivation and stabilization of RUNX3. These compounds represented the three different groups involved in RUNX transcriptional activation (**7j**, group I with strong HDAC inhibition; **7c**, group II with mild HDAC inhibition; and **7k**, group III with mild HDAC inhibition).

Female S.P.F BALB/c nude mice were injected subcutaneously (s.c.) with 4×10^7 cells/mL (MKN28 cell line) before treatment with oral feeding once a day for 2 weeks with 10 mL/kg (30 mg/kg) for each compound. Three compounds (**7c**, **7j**, and **7k**) were considered to be relatively nontoxic because of good animal survival and no loss of weight (Fig. 3A). The **7k** compound showed significantly decreased the tumor weight by 43.7% compared to **7c** and **7j**. (20.2%, and 12.4%, respectively; Table 3). Compound **7k** showed 111.0% RUNX transcriptional activation (group III) and mild HDAC inhibition, while **7c** and **7j** showed 164.8% and 324.9% RUNX transcriptional activity with mild and strong HDAC inhibition, respectively. It seems that strong HDAC inhibitors with lower activity to restore the RUNX3 protein showed poor *in vivo* efficacy. This selective stabilization of RUNX3 stabilization over nonspecific gene expression was an important factor in tumor suppression. Furthermore, **7k** showed greater metabolic stability compared with

Table 2
Microsomal stability of pyridone-based analogues.

Cpd	linker	R	% remaining after 30 min	
			(-) NADPH	(+) NADPH
4l^a	alkyl	2-Bromophenyl	93.3 ± 0.0	24.2 ± 0.0
4m^a	alkyl	3-Bromophenyl	96.7 ± 0.0	20.7 ± 0.0
4q^b	alkyl	2-Naphthyl	90.3 ± 4.5	35.5 ± 2.7
4r	alkyl	Phenyl	95.35 ± 1.64	65.10 ± 0.74
7b	olefin	2-Bromophenyl	93.28 ± 2.47	33.61 ± 1.31
7c	olefin	3-Bromophenyl	89.93 ± 4.29	40.91 ± 1.27
7i	olefin	2-Naphthyl	89.57 ± 1.69	27.93 ± 0.35
7j	olefin	2-Quinoliny	82.80 ± 1.46	65.84 ± 4.10
7k	olefin	Phenyl	99.12 ± 3.09	88.21 ± 1.05
buspirone			99.07 ± 1.39	0.29 ± 0.11

^a Compounds were reported in our previous work [30].

^b Compounds from reported in our previous work [22].

2.7. Pharmacokinetics profiling

Based on the results of metabolic stability profiles and *in vivo* pharmacokinetic studies, compound **7k** was selected for *in vivo* pharmacokinetic evaluation (Table 4). Compound **7k** was administered intravenously and orally at 2 and 10 mg/kg, respectively, in male ICR mice. The plasma concentration profile of **7k** showed a peak plasma concentration of C_{max} (627.0 ± 360.9 ng/mL) and T_{max} (18 min) using oral administration. The AUC_{inf} (Area Under the Curve) values of **7k** from the intravenous and oral administrations were 496.3 ± 53.2 ng/h/mL and 1350.8 ± 291.7 ng/h/mL, respectively. The

clearance and steady state volume of **7k** during intravenous administration were 4.1 ± 0.5 l/h/kg and 11.4 ± 2.6 l/kg, respectively. The terminal half-lives of **7k** were approximately 3.4 h and 5.2 h after intravenous and oral dosing, respectively. The oral bioavailability for **7k** was 54.4%. These results were consistent with the pharmacological effects of **7k** in the xenograft regression model, and strongly suggested that compound **7k** could be an effective orally administered anti-cancer agent.

3. Conclusions

We report a new series of pyridone-based RUNX3 modulators with an alkenyl group connecting to a cap group that was shown to improve the biological potency and pharmacokinetic profiles. Twenty-two pyridone-based analogues were synthesized and evaluated using various biological assays. All compounds with the alkenyl linker between the cap group and core structures showed improved activities for HDAC inhibition, RUNX3 transcriptional activation, and cancer cell growth inhibition compared to those with one alkyl linker. The ratio of Ac-RUNX3/Ac-histone (H3) was also estimated to determine the selectivity of RUNX3 stabilization compared with nonspecific gene expression. This could be an important factor for antitumor activity through RUNX3 modulation. Among the alkenyl compounds, **7i** and **7k** showed the best ratio of Ac-RUNX3/Ac-histone at 4.3 and 3.8, respectively. The metabolic stability profiles showed that the alkenyl linker analogues had better stability than the alkyl linker analogues. Based on the results of the *in vitro* assays, three compounds were selected to

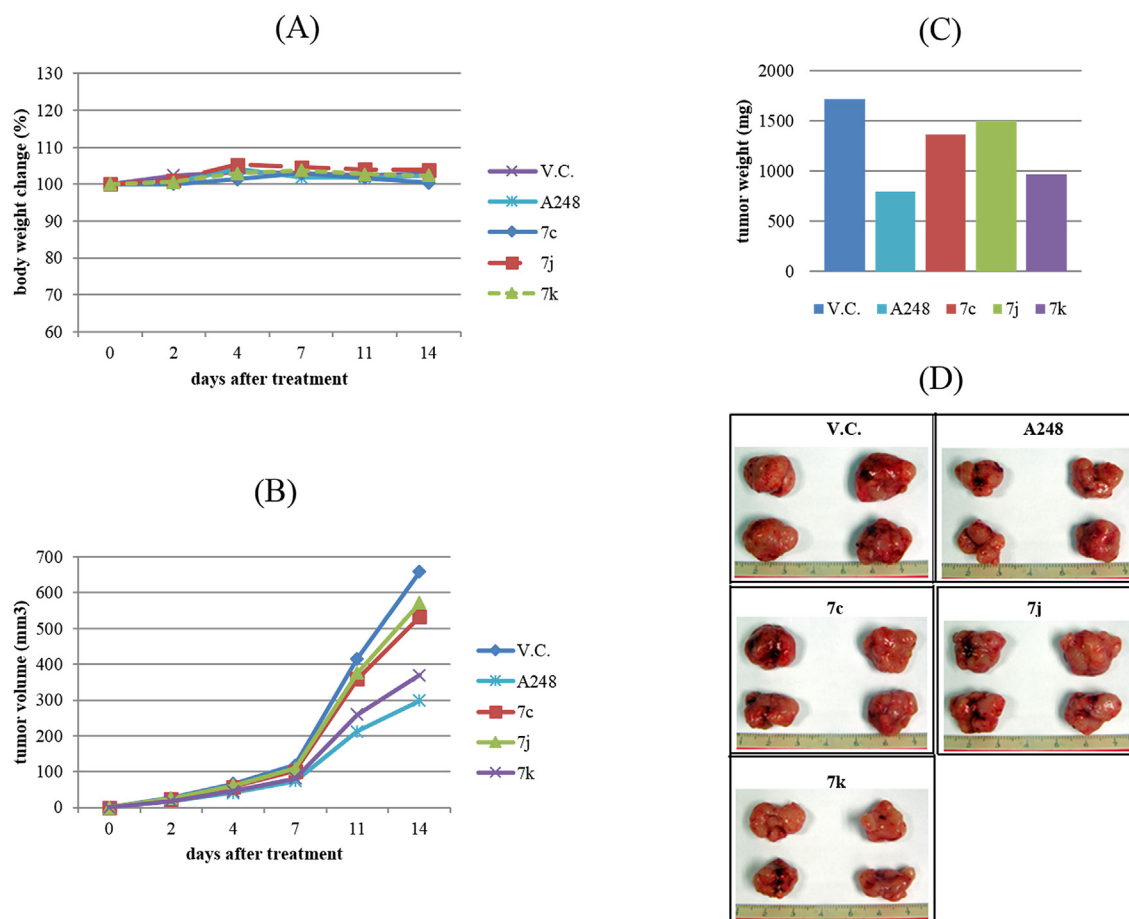


Fig. 3. *In vivo* study of the human stomach tumor (MKN28) xenograft regression model.

Table 3
Effect of **7k**, **7c**, and **7j**, 30 mg/kg, 4×10^7 cells/ml on the growth of a human stomach tumor (MKN28) xenograft regression model.

Group (n = 4)	Dose (mg/kg)	Tumor volume ^{(Vt-Vo)†}						Tumor weight (mg)
		day 0	2	4	7	11	14	14
		-124	-126	-128	-131	-204	-207	-207
Vehicle Control (D10 + T10 + D80%)	0	0 ±0.0	25.9 ±5.3	65.9 ±10.6	118.1 ±9.9	415.5 ±54.3	659.1 ±61.1	1716 ±223.7
7k	30	0 ±0.0	18.3 ±2.8 *	45.2 ±5.8 *	80.1 ±7.1 ***	260.1 ±24.4 **	369.2 ±46.2 ***	965.6 ±97.2 ***
7c	30	0 ±0.0	29.30% 22.3 ±7.1	31.40% 57.3 ±9.9	32.20% 101.3 ±14.9	37.40% 359.3 ±27.9	44.00% 533.4 ±75.0 *	43.70% 1368.8 ±85.4 *
7j	30	0 ±0.0	13.80% 25.2 ±5.4	12.90% 61.4 ±11.7	14.30% 108.7 ±18.4	13.50% 375.7 ±12.0	19.10% 570.9 ±25.9 *	20.20% 1503.2 ±179.1
A248	30	0 ±0.0	2.80% 16.5 ±3.0 *	6.80% 40.8 ±4.6 **	8.00% 73.8 ±7.1 ***	9.60% 212.2 ±21.9 ***	13.40% 298 ±21.8 ***	12.40% 794.6 ±81.7 ***
			36.40%	38.00%	37.60%	48.90%	54.80%	53.70%

Significant figures (t-TEST) : *p < 0.05, **p < 0.01, ***p < 0.001 vs Vehicle Control.
† : $\Delta t = Vt - Vo$, Vt (Measurement of the tumor volume), Vo (Initial tumor volume).

treat mice to monitor the antitumor effects of a human gastric tumor (MKN28) xenograft regression model. When the mice were treated with **7k** (R, phenyl; olefin linker; moderate HDAC inhibitory activity, and group II in RUNX transcriptional activity), a significant *in vivo* antitumor activity was observed. In experiments, the results consistently provide that the *in vivo* efficacy is quite related to RUNX3 stability with weak or moderate activation of RUNX3 when the xenograft experiments using MKN28 which are RUNX3-off cells. Based on our results, strong HDAC inhibitors with lower activity to restore the RUNX3 protein showed poor *in vivo* efficacy. The **7k** compound also showed a long half-life (3.4 h and 5.2 h after intravenous and oral dosing, respectively) and potent oral bioavailability (54.4%) using an *in vivo* pharmacokinetic study. By modulation of RUNX3 activity, the results strongly suggested that **7k** could be a highly potent and orally available anticancer chemotherapeutic agent.

Table 4
Oral (PO) and intravenous (IV) pharmacokinetic parameters of **7k** in male ICR mice.

PK parameter ^a		IV			PO		
		mean	SD	n	mean	SD	n
Dose	(mg/kg)	2		3	10		3
t_{max}	(hr)	NA			0.3	0.0	3
C_{max}	(ng/ml)	NA			627.0	360.9	3
AUC_{inf}^b	(ng.hr/ml)	496.3	53.2	3	1350.8	291.7	3
CL	(l/hr/kg)	4.1	0.5	3	NA		
V_{ss}	(l/kg)	11.4	2.6	3	NA		
t_{1/2}	(hr)	3.4	0.2	3	5.2	1.6	3
F	(%)	NA			54.4	11.8	3

^a PK parameters were based on mean plasma concentration–time profiles of three animals per time points. PK parameters were calculated by non-compartmental analysis using PK Solutions 2.0 (Summit Research Services, Montrose, CO, USA).

^b AUC after intravenous (iv) administration was calculated from 0 to infinity, whereas the oral AUC was calculated from 0 to 5 h. Since the purpose of this study is to find orally available anticancer reagent, the bioavailability of the compound is considered to be important because it shows potential of this compound to be orally administered. Therefore, it was bolded to give an emphasis.

4. Experimental

4.1. Chemistry

4.1.1. Experimental section

All chemicals were obtained from commercial suppliers and used without further purification. All reactions were monitored by thin-layer chromatography (TLC) on pre-coated silica gel 60 F254 (mesh) (E. Merck, Mumbai, India), and spots were visualized under UV light (254 nm). Flash column chromatography was performed with silica (Merck EM9385, 230–400 mesh). ¹H and ¹³C nuclear magnetic resonance (NMR, Varan Unity Inova) spectra were recorded at 400 and 100 MHz, or at 500 and 125 MHz. Proton and carbon chemical shifts are expressed in ppm relative to internal tetramethylsilane, and coupling constants (J) are expressed in Hertz. Splitting patterns were presented as s, singlet; d, doublet; t, triplet; q, quartet; dd, double of doublets; dt, double of triplet; m, multiplet; br, broad. LC–MS (Liquid chromatography–mass spectrometry) spectra were recorded by electrospray ionization (ESI) probe using a Shimadzu LC–MS2010 instrument with an Agilent C18 column, 50*4.6mm, 5 μm particle size; mobile phase: 0.1% formic acid in H₂O/0.1% formic acid in CH₃CN (1:9) over 10 min; flow rate: 0.2 mLmin⁻¹; scan mode (0–500 amuz⁻¹). The detected ion peaks were (M + z)/z in positive where M represents the molecular weight of the compound and z represents the charge (number of protons). High-resolution ESI–MS measurements were performed on a Micromass Quadrupole–Time of Flight (Q–TOF) Acuity UPLC–Mass System at Yonsei University; positive mode.

4.1.2. General procedure for **3** and **6**

A solution of (*E*)-methyl 3-(2-oxo-1,2-dihydropyridin-3-yl)acrylate **1** (0.2 g, 1.12 mmol) in acetone (0.2 m) was added to alkyl halide **2** or alkenyl halide **5** (1.67 mmol) in the presence of K₂CO₃ (0.46 g, 3.35 mmol). The reaction mixture was stirred at reflux for 12 h, then was diluted with acetone, filtered over a Celite pad to remove K₂CO₃, and concentrated. The crude product was purified by flash column chromatography (EtOAc/CH₂Cl₂, 1:5–1:1).

4.1.2.1. (*E*)-methyl 3-(2-oxo-1-(3-(2-(trifluoromethyl)phenyl)propyl)-1,2-dihydropyridin-3-yl)acrylate (**3a**). Brown oil (212 mg, 57.0%). ^1H NMR (500 MHz, DMSO- d_6) δ 8.13 (d, 1H, J = 5.0 Hz), 7.64–7.28 (m, 3H), 7.16 (d, 1H, J = 12.5 Hz), 7.11 (d, 1H, J = 3.5 Hz), 6.75 (td, 1H, J_A = 55.0 Hz, J_B = 5.5 Hz), 6.23 (t, 1H, J = 6.5 Hz), 6.00 (d, 1H, J = 13.0 Hz), 4.14–4.09 (m, 2H), 3.77 (s, 3H), 2.84 (t, 2H, J = 7.5 Hz), 2.11–2.09 (m, 2H); ^{13}C NMR (125 MHz, DMSO- d_6) δ 168.2, 160.8, 140.8, 140.3, 138.7, 138.5, 138.2, 131.9, 130.8, 130.0, 126.5, 126.3, 125.7, 120.4, 105.8, 51.5, 51.3, 30.7, 21.0; ESI (m/z) 366 (MH^+), 388 (MNa^+).

4.1.2.2. (*E*)-methyl 3-(2-oxo-1-(3-(3-(trifluoromethyl)phenyl)propyl)-1,2-dihydropyridin-3-yl)acrylate (**3b**). Yellow oil (154 mg, 50.3%). ^1H NMR (500 MHz, DMSO- d_6) δ 7.99–7.81 (m, 2H), 7.60–7.32 (m, 5H), 7.13 (d, 1H, J = 16.0 Hz), 6.28 (t, 1H, J = 6.5 Hz), 3.98 (t, 2H, J = 8.0 Hz), 3.71 (s, 3H), 2.71 (t, 2H, J = 7.5 Hz), 2.02–1.94 (m, 2H); ^{13}C NMR (125 MHz, DMSO- d_6) δ 168.0, 161.1, 140.4, 140.0, 138.2, 138.0, 137.6, 131.5, 130.2, 129.6, 126.7, 126.4, 125.8, 120.6, 105.2, 51.1, 50.4, 30.5, 20.7; ESI (m/z) 366 (MH^+), 388 (MNa^+).

4.1.2.3. (*E*)-methyl 3-(2-oxo-1-(3-(4-(trifluoromethyl)phenyl)propyl)-1,2-dihydropyridin-3-yl)acrylate (**3c**). Brown oil (224 mg, 71.8%). ^1H NMR (500 MHz, DMSO- d_6) δ 8.13 (d, 1H, J = 7.0 Hz), 7.62 (d, 1H, J = 16.0 Hz), 7.54–7.52 (m, 2H), 7.31–7.24 (m, 2H), 7.12 (dd, 1H, J_A = 13.0 Hz, J_B = 3.5 Hz), 6.28 (t, 1H, J = 8.5 Hz), 6.01 (d, 1H, J = 13.0 Hz), 3.99 (t, 2H, J = 8.0 Hz), 3.77 (s, 3H), 2.75 (t, 2H, J = 7.0 Hz), 2.14–2.11 (m, 2H); ^{13}C NMR (125 MHz, DMSO- d_6) δ 166.6, 161.4, 140.8, 140.2, 138.7, 138.4, 138.2, 128.6(3), 125.4(2), 119.9, 105.7, 51.6, 49.9, 32.6, 30.1; ESI (m/z) 366 (MH^+), 388 (MNa^+).

4.1.2.4. (*E*)-methyl 3-(1-(3-(2-chlorophenyl)propyl)-2-oxo-1,2-dihydropyridin-3-yl)acrylate (**3d**). Yellow oil (130 mg, 83.2%). ^1H NMR (500 MHz, CDCl_3) δ 7.63 (d, 1H, J = 16.0 Hz), 7.52 (dd, 1H, J_A = 7.25 Hz, J_B = 2.5 Hz), 7.34–7.32 (m, 1H), 7.30–7.28 (m, 1H), 7.24 (dt, 1H, J_A = 7.5 Hz, J_B = 4.0 Hz), 7.19 (dd, 1H, J_A = 7.25 Hz, J_B = 1.0 Hz), 7.16–7.15 (m, 1H), 7.11 (d, 1H, J = 15.5 Hz), 6.23 (q, 1H, J_A = 7.0 Hz, J_B = 4.0 Hz), 4.06–3.99 (m, 2H), 3.74 (d, 3H, J = 36.0 Hz), 2.82–2.79 (m, 2H), 2.14–2.08 (m, 2H); ESI (m/z) 332 (MH^+), 354 (MNa^+).

4.1.2.5. (*E*)-methyl 3-(1-(3-(3-chlorophenyl)propyl)-2-oxo-1,2-dihydropyridin-3-yl)acrylate (**3e**). Yellow oil (907.5 mg, 47.8%). ^1H NMR (400 MHz, DMSO- d_6) δ 7.89–7.85 (m, 2H), 7.60 (d, 1H, J = 15.6 Hz), 7.33–7.19 (m, 4H), 7.07 (d, 1H, J = 16.0), 6.36 (t, 1H, J = 6.8 Hz), 4.00 (t, 2H, J = 7.4 Hz), 3.71 (s, 3H), 2.64 (t, 2H, J = 7.6 Hz), 2.02–1.95 (m, 2H); ^{13}C NMR (100 MHz, DMSO- d_6) δ 167.7, 160.4, 144.0, 142.4, 141.3, 141.2, 133.3, 130.5, 128.4, 27.3, 126.3, 123.5, 118.8, 105.9, 51.7, 49.1, 32.1, 30.2; ESI (m/z) 355 (MNa^+).

4.1.2.6. (*E*)-methyl 3-(1-(3-(4-chlorophenyl)propyl)-2-oxo-1,2-dihydropyridin-3-yl)acrylate (**3f**). Yellow oil (1.4 mg, 5.6%). ^1H NMR (400 MHz, DMSO- d_6) δ 7.89–7.85 (m, 2H), 7.59 (d, 1H, J = 15.6 Hz), 7.33 (d, 2H, J = 8.4 Hz), 7.25 (d, 2H, J = 8.4 Hz), 7.06 (d, 1H, J = 15.6 Hz), 6.36 (t, 1H, J = 15.6), 3.98 (t, 2H, J = 15.6 Hz), 3.70 (s, 3H), 2.61 (t, 2H, J = 7.8 Hz), 2.00–1.92 (m, 2H); ^{13}C NMR (100 MHz, DMSO- d_6) δ 167.7, 160.4, 142.4, 141.4, 141.2, 140.4, 130.9, 130.5 (2), 128.6 (2), 123.5, 118.8, 105.9, 51.7, 49.2, 31.8, 30.3; ESI (m/z) 332 (MH^+), 354 (MNa^+).

4.1.2.7. (*E*)-methyl 3-(1-(3-(2-methoxyphenyl)propyl)-2-oxo-1,2-dihydropyridin-3-yl)acrylate (**3g**). Brown oil (154 mg, 94.4%). ^1H NMR (500 MHz, DMSO- d_6) δ 7.47 (d, 1H, J = 12.5 Hz), 7.45–7.39 (m, 2H), 7.25 (d, 1H, J = 15.0 Hz), 7.10–7.07 (m, 2H), 7.01–6.97 (m, 2H), 6.65 (d, 1H, J = 7.5 Hz), 3.95 (t, 2H, J = 7.5 Hz), 3.73 (d, 6H, J = 11.5 Hz), 2.55 (t, 2H, J = 7.5 Hz), 2.10–2.05 (m, 2H); ESI (m/z) 328

(MH^+), 350 (MNa^+).

4.1.2.8. (*E*)-methyl 3-(1-(3-(naphthalen-1-yl)propyl)-2-oxo-1,2-dihydropyridin-3-yl)acrylate (**3h**). Yellow oil (34.2 mg, 90.9%). ^1H NMR (500 MHz, DMSO- d_6) δ 8.01 (d, 1H, J = 8.0 Hz), 7.93–7.88 (m, 2H), 7.76 (d, 1H, J = 8.0 Hz), 7.60 (d, 1H, J = 16.0 Hz), 7.54–7.48 (m, 2H), 7.43–7.37 (m, 2H), 7.07 (d, 1H, J = 16.0 Hz), 6.37 (t, 1H, J = 6.8 Hz), 5.99 (d, 1H, J = 13.0 Hz), 4.11 (t, 2H, J = 7.2 Hz), 3.69 (s, 3H), 3.09–3.05 (m, 2H), 2.09–2.03 (m, 2H); ^{13}C NMR (125 MHz, CDCl_3) δ 168.0, 166.8, 161.1, 160.8, 142.8, 141.8, 141.6, 137.9, 134.2, 132.0, 129.3, 127.3, 126.7, 126.3, 124.2, 119.2, 106.3, 52.1, 51.8, 50.0, 30.4, 29.9; ESI (m/z) 348 (MH^+), 370 (MNa^+).

4.1.2.9. (*E*)-methyl 3-(2-oxo-1-(3-(2-(trifluoromethoxy)phenyl)propyl)-1,2-dihydropyridin-3-yl)acrylate (**3i**). Yellow oil (34.2 mg, 90.9%). ^1H NMR (500 MHz, CDCl_3) δ 8.04–8.02 (m, 1H), 7.53–7.41 (m, 1H), 7.40–7.23 (m, 2H), 7.21 (dd, 1H, J_A = 9.0 Hz, J_B = 4.5 Hz), 7.19–7.16 (m, 2H), 7.06–7.02 (m, 3H), 6.13–6.08 (m, 1H), 3.92–3.85 (m, 2H), 3.64 (s, 3H), 2.63 (t, 2H, J = 8.0 Hz), 1.97 (d, 2H, J = 5.5 Hz); ESI (m/z) 382 (MH^+), 404 (MNa^+).

4.1.2.10. (*E*)-methyl 3-(2-oxo-1-(3-(3-(trifluoromethoxy)phenyl)propyl)-1,2-dihydropyridin-3-yl)acrylate (**3j**). Yellow oil (96.8 mg, 12.76%). ^1H NMR (400 MHz, DMSO- d_6) δ 7.87 (t, 2H, J = 5.2 Hz), 7.59 (d, 1H, J = 15.6 Hz), 7.31 (d, 4H, J = 8.4 Hz), 7.07 (d, 1H, J = 16.0 Hz), 6.36 (t, 1H, J = 6.8 Hz), 4.2 (t, 2H, J = 7.2 Hz), 3.71 (s, 3H), 2.66 (t, 2H, J = 7.6 Hz), 2.03–1.95 (m, 2H); ^{13}C NMR (100 MHz, DMSO- d_6) δ 167.7, 160.5, 147.0, 142.5, 141.4, 141.2, 141.0, 130.4(3), 123.6, 121.3(2), 118.9, 106.0, 51.8, 49.2, 31.9, 30.3; ESI (m/z) 382 (MH^+), 404 (MNa^+).

4.1.2.11. (*E*)-methyl 3-(2-oxo-1-(3-(4-(trifluoromethoxy)phenyl)propyl)-1,2-dihydropyridin-3-yl)acrylate (**3k**). Yellow oil (100 mg, 50.1%). ^1H NMR (500 MHz, CDCl_3) δ 7.54 (d, 1H, J = 16.0 Hz), 7.43 (dd, 1H, J_A = 7.0 Hz, J_B = 1.5 Hz), 7.22–7.18 (m, 2H), 7.18–7.12 (m, 2H), 7.04 (q, 2H, J_A = 9.0 Hz, J_B = 17.5 Hz), 6.13 (q, 1H, J_A = 7.0 Hz, J_B = 14.0 Hz), 3.90 (dt, 2H, J_A = 19.0 Hz, J_B = 7.5 Hz), 3.69 (s, 3H), 2.63–2.60 (m, 2H), 2.04–2.00 (m, 2H); ESI (m/z) 382 (MH^+), 404 (MNa^+).

4.1.2.12. (*E*)-methyl 3-(2-oxo-1-((*E*)-3-(3-(trifluoromethyl)phenyl)allyl)-1,2-dihydropyridin-3-yl)acrylate (**6a**). Yellow oil (270 mg, 21.7%). ^1H NMR (500 MHz, CDCl_3) δ 7.65 (d, 1H, J = 16.0 Hz), 7.61 (s, 1H), 7.58–7.54 (m, 2H), 7.51 (d, 1H, J = 8.0 Hz), 7.45–7.41 (m, 2H), 7.14 (d, 1H, J = 15.5 Hz), 6.63 (d, 1H, J = 16.0 Hz), 6.45–6.39 (m, 1H), 6.30 (t, 1H, J = 7.0 Hz), 4.80 (dd, 2H, J_A = 6.0 Hz, J_B = 1.0 Hz), 3.79 (s, 3H); ^{13}C NMR (125 MHz, CDCl_3) δ 168.4, 160.9, 141.3, 140.4, 138.3, 136.9, 133.0, 130.0, 129.4, 125.9, 125.5, 125.0, 123.6, 120.9, 106.4, 51.8, 51.5; ESI (m/z) 364 (MH^+), 386 (MNa^+).

4.1.2.13. (*E*)-methyl 3-(1-((*E*)-3-(2-bromophenyl)allyl)-2-oxo-1,2-dihydropyridin-3-yl)acrylate (**6b**). Yellow oil (260 mg, 36.5%). ^1H NMR (500 MHz, CDCl_3) δ 7.64–7.61 (m, 1H), 7.53–7.43 (m, 4H), 7.24–7.21 (m, 1H), 7.14–7.07 (m, 2H), 6.93 (d, 1H, J = 16.0 Hz), 6.30–6.23 (m, 2H), 4.79 (dd, 2H, J_A = 5.5 Hz, J_B = 1.0 Hz), 3.76–3.75 (m, 3H); ^{13}C NMR (125 MHz, CDCl_3) δ 167.7, 160.3, 142.7, 141.1(2), 135.7, 133.2, 131.0, 130.1, 128.4, 128.4, 127.7, 123.2, 119.1, 106.3, 51.8, 50.7; ESI (m/z) 374 (MH^+), 396 (MNa^+).

4.1.2.14. (*E*)-methyl 3-(1-((*E*)-3-(3-bromophenyl)allyl)-2-oxo-1,2-dihydropyridin-3-yl)acrylate (**6c**). Yellow oil (200 mg, 38.2%). ^1H NMR (500 MHz, CDCl_3) δ 7.66–7.62 (m, 1H), 7.55 (dd, 1H, J_A = 5.0 Hz, J_B = 2.0 Hz), 7.50 (br t, 1H, J = 2.0 Hz), 7.42–7.39 (m, 1H), 7.38–7.36 (m, 1H), 7.28–7.27 (m, 1H), 7.19–7.11 (m, 2H), 6.52 (d, 1H, J = 16.0 Hz), 6.35–6.26 (m, 2H), 4.77–4.76 (m, 2H), 3.78–3.77 (m,

3H); ^{13}C NMR (125 MHz, CDCl_3) δ 167.7, 160.3, 142.7, 141.2, 141.1, 138.9, 131.6, 131.1, 130.9, 129.4, 126.8, 125.9, 123.8, 122.6, 119.0, 106.3, 51.8, 50.6; ESI (m/z) 374 (MH^+), 396 (MNa^+).

4.1.2.15. (*E*)-methyl 3-(1-((*E*)-3-(4-bromophenyl)allyl)-2-oxo-1,2-dihydropyridin-3-yl)acrylate (**6d**). Yellow oil (100 mg, 22.1%). ^1H NMR (500 MHz, CDCl_3) δ 7.64 (dd, 1H, $J_A = 16.0$ Hz, $J_B = 0.5$ Hz), 7.55 (dd, 1H, $J_A = 5.5$ Hz, $J_B = 2.0$ Hz), 7.24–7.22 (m, 2H), 7.13 (d, 1H, $J = 16.0$ Hz), 6.54 (d, 1H, $J = 15.5$ Hz), 6.35–6.27 (m, 2H), 4.76 (dd, 2H, $J_A = 5.0$ Hz, $J_B = 1.5$ Hz), 3.79 (s, 3H); ^{13}C NMR (125 MHz, CDCl_3) δ 167.7, 160.34, 142.7, 141.2, 141.1, 135.7, 132.0, 131.9(2), 128.9(2), 125.9, 123.8, 121.3, 119.0, 106.3, 51.8, 50.71; ESI (m/z) 374 (MH^+), 396 (MNa^+).

4.1.2.16. (*E*)-methyl 3-(1-((*E*)-3-(3-chlorophenyl)allyl)-2-oxo-1,2-dihydropyridin-3-yl)acrylate (**6e**). Yellow oil (470 mg, 33.3%). ^1H NMR (500 MHz, CDCl_3) δ 7.63 (d, 1H, $J = 15.5$ Hz), 7.54 (d, 1H, $J = 7.0$ Hz), 7.40 (d, 1H, $J = 7.0$ Hz), 7.33 (s, 1H), 7.21 (s, 3H), 7.12 (d, 1H, $J = 15.5$ Hz), 6.52 (d, 1H, $J = 15.5$ Hz), 6.35–6.26 (m, 2H), 4.76 (d, 2H, $J = 6.5$ Hz), 3.77 (s, 3H); ^{13}C NMR (125 MHz, CDCl_3) δ 168.4, 160.9, 141.3, 140.4, 138.4, 137.9, 134.8, 133.1, 130.1, 128.3, 126.7, 125.7, 125.0, 120.747, 106.4, 51.8, 51.4; ESI (m/z) 330 (MH^+), 352 (MNa^+).

4.1.2.17. (*E*)-methyl 3-(1-((*E*)-3-(3-methoxyphenyl)allyl)-2-oxo-1,2-dihydropyridin-3-yl)acrylate (**6f**). Orange oil (380 mg, 24.6%). ^1H NMR (500 MHz, CDCl_3) δ 7.64 (d, 1H, $J = 15.5$ Hz), 7.54 (dd, 1H, $J_A = 6.0$ Hz, $J_B = 1.0$ Hz), 7.42 (dd, 1H, $J_A = 5.5$ Hz, $J_B = 1.5$ Hz), 7.22 (t, 1H, $J = 7.5$ Hz), 7.15–7.10 (m, 1H), 6.96 (d, 1H, $J = 8.0$ Hz), 6.90 (s, 1H), 6.83–6.80 (m, 1H), 6.59 (d, 1H, $J = 16.0$ Hz), 6.34–6.25 (m, 2H), 4.76 (d, 2H, $J = 6.5$ Hz), 3.79 (s, 3H), 3.78 (s, 3H); ^{13}C NMR (125 MHz, CDCl_3) δ 168.2, 160.7, 159.8, 141.0, 140.3, 138.1, 137.3, 134.5, 129.6, 125.5, 123.4, 120.5, 119.3, 114.057, 111.7, 106.0, 55.3, 51.6, 51.1; ESI (m/z) 326 (MH^+), 348 (MNa^+).

4.1.2.18. (*E*)-methyl 3-(2-oxo-1-((*E*)-3-(3-(trifluoromethoxy)phenyl)allyl)-1,2-dihydropyridin-3-yl)acrylate (**6g**). Yellow solid (500 mg, 48.1%). ^1H NMR (500 MHz, CDCl_3) δ 7.63 (d, 1H, $J = 15.5$ Hz), 7.55 (dd, 1H, $J_A = 5.0$ Hz, $J_B = 2.0$ Hz), 7.41 (dd, 1H, $J_A = 4.5$ Hz, $J_B = 2.0$ Hz), 7.34–7.28 (m, 2H), 7.20 (s, 1H), 7.13 (d, 1H, $J = 15.5$ Hz), 7.11–7.08 (m, 1H), 6.57 (d, 1H, $J = 16.0$ Hz), 6.35 (dt, 1H, $J_A = 15.5$ Hz, $J_B = 6.5$ Hz), 6.28 (t, 1H, $J = 6.5$ Hz), 4.77 (dd, 2H, $J_A = 5.0$ Hz, $J_B = 1.5$ Hz), 3.77 (s, 3H); ^{13}C NMR (125 MHz, CDCl_3) δ 168.1, 160.6, 149.6, 141.0, 140.1, 138.1, 138.0, 132.8, 130.0, 125.6, 125.1, 125.0, 120.6, 120.4, 119.4, 118.9, 106.2, 51.6, 51.1; ESI (m/z) 380 (MH^+), 402 (MNa^+).

4.1.2.19. (*E*)-methyl 3-(1-((*E*)-3-(naphthalen-1-yl)allyl)-2-oxo-1,2-dihydropyridin-3-yl)acrylate (**6h**). Yellow oil (90 mg, 5.8%). ^1H NMR (500 MHz, CDCl_3) δ 8.06 (d, 1H, $J = 8.0$ Hz), 7.85 (d, 1H, $J = 8.0$ Hz), 7.79 (d, 1H, $J = 8.5$ Hz), 7.67 (d, 1H, $J = 16.0$ Hz), 7.59 (d, 1H, $J = 7.0$ Hz), 7.54 (t, 2H, $J = 6.5$ Hz), 7.51–7.48 (m, 2H), 7.43 (t, 1H, $J = 8.0$ Hz), 7.39 (d, 1H, $J = 15.5$ Hz), 7.16 (dd, 1H, $J_A = 15.5$ Hz, $J_B = 0.5$ Hz), 6.38–6.32 (m, 1H), 6.30–6.27 (m, 1H), 4.89 (d, 2H, $J = 6.5$ Hz), 3.79 (s, 3H); ^{13}C NMR (125 MHz, CDCl_3) δ 168.2, 160.7, 141.0, 140.3, 138.1, 133.6, 133.5, 131.9, 131.0, 128.6, 128.565, 126.3, 125.9, 125.5, 124.2, 123.5, 120.5, 106.1, 51.6, 51.3; ESI (m/z) 346 (MH^+), 368 (MNa^+).

4.1.2.20. (*E*)-methyl 3-(1-((*E*)-3-(naphthalen-2-yl)allyl)-2-oxo-1,2-dihydropyridin-3-yl)acrylate (**6i**). Yellow solid (70 mg, 7.7%). ^1H NMR (500 MHz, CDCl_3) δ 7.80–7.79 (m, 2H), 7.75 (d, 2H, $J = 15.5$ Hz), 7.70–7.66 (m, 1H), 7.59–7.54 (m, 2H), 7.48–7.43 (m, 3H), 7.19–7.15 (m, 1H), 6.77 (d, 1H, $J = 16.0$ Hz), 6.48–6.42 (m, 1H), 6.28–6.25 (m, 1H), 4.82 (d, 2H, $J = 6.5$ Hz), 3.81–3.80 (m, 3H); ESI (m/z) 346 (MH^+), 368 (MNa^+).

4.1.2.21. (*E*)-methyl 3-(2-oxo-1-((*E*)-3-(quinolin-2-yl)allyl)-1,2-dihydropyridin-3-yl)acrylate (**6j**). Red solid (2.12 g, 97.1%). ^1H NMR (500 MHz, CDCl_3) δ 8.16 (d, 1H, $J = 8.5$ Hz), 8.06 (d, 1H, $J = 8.5$ Hz), 7.81 (d, 1H, $J = 8.0$ Hz), 7.73 (d, 2H, $J = 7.0$ Hz), 7.64 (d, 1H, $J = 16.0$ Hz), 7.56–7.54 (m, 3H), 7.11 (d, 1H, $J = 16.0$ Hz), 6.29 (t, 1H, $J = 7.0$ Hz), 5.49 (s, 2H), 3.77 (s, 3H); ESI (m/z) 347 (MH^+), 349 (MNa^+).

4.1.2.22. (*E*)-methyl 3-(1-cinnamyl-2-oxo-1,2-dihydropyridin-3-yl)acrylate (**6k**). Yellow oil (420 mg, 93.5%). ^1H NMR (500 MHz, CDCl_3) δ 8.09 (dd, 1H, $J_A = 7.0$ Hz, $J_B = 1.5$ Hz), 7.46 (dd, 1H, $J_A = 7.0$ Hz, $J_B = 1.5$ Hz), 7.34 (dd, 1H, $J_A = 6.5$ Hz, $J_B = 2.0$ Hz), 7.31 (d, 1H, $J = 2.0$ Hz), 7.30–7.24 (m, 2H), 7.21 (t, 2H, $J = 7.5$ Hz), 7.15–7.11 (m, 1H), 6.53 (dd, 1H, $J_A = 16.0$ Hz, $J_B = 5.0$ Hz), 6.27–6.15 (m, 2H), 4.70–4.65 (m, 2H), 3.70 (s, 3H); ^{13}C NMR (125 MHz, CDCl_3) δ 168.4, 160.9, 141.1, 140.4, 138.3, 136.0, 134.8, 128.8, 128.4, 126.8, 125.6, 123.3, 120.6, 106.202, 51.8, 51.4; ESI (m/z) 296 (MH^+), 318 (MNa^+).

4.1.3. General procedure for **4** and **7**

NH_2OK (1.7 m suspension in MeOH, 1.6 mL) was added to a solution of **3** or **6** (0.14 mmol) in anhydrous MeOH (0.2 mL), and the mixture was stirred for 12 h at 0 °C. The mixture was concentrated, and the crude product was purified by flash column chromatography (5–10% MeOH in CH_2Cl_2).

4.1.3.1. (*E*)-*N*-hydroxy-3-(2-oxo-1-(3-(2-(trifluoromethyl)phenyl)propyl)-1,2-dihydropyridin-3-yl)acrylamide (**4a**). Light brown solid (80 mg, 40%). MP: 45–48 °C; ^1H NMR (500 MHz, $\text{DMSO}-d_6$) δ 7.82 (d, 1H, $J = 6.5$ Hz), 7.83–7.35 (m, 6H), 7.13 (d, 1H, $J = 15.0$ Hz), 6.30 (dt, 1H, $J_A = 34.0$ Hz, $J_B = 7.0$ Hz), 4.04 (dt, 2H, $J = 27.0$ Hz, 7.5 Hz), 2.77 (t, 2H, $J = 7.5$ Hz), 1.97 (q, 2H, $J = 7.5$ Hz); ESI (m/z) 367 (MH^+), 389 (MNa^+); HRMS (ESI) calculated for $\text{C}_{18}\text{H}_{17}\text{F}_3\text{N}_2\text{O}_3$ (MH^+), found.

4.1.3.2. (*E*)-*N*-hydroxy-3-(2-oxo-1-(3-(3-(trifluoromethyl)phenyl)propyl)-1,2-dihydropyridin-3-yl)acrylamide (**4b**). Brown solid (46 mg, 47.4%). MP: 135–137 °C; ^1H NMR (500 MHz, $\text{DMSO}-d_6$) δ 7.78 (d, 1H, $J = 4.0$ Hz), 7.72–7.60 (m, 3H), 7.47 (d, 2H, $J = 7.0$ Hz), 7.37 (t, 1H, $J = 9.0$ Hz), 7.12–6.77 (m, 1H), 6.29 (dt, 1H, $J_A = 42.0$ Hz, $J_B = 6.0$ Hz), 3.98 (dt, 2H, $J_A = 26.0$ Hz, $J_B = 7.0$ Hz), 2.73 (t, 2H, $J = 8.5$ Hz), 2.04–1.97 (m, 2H); ESI (m/z) 367 (MH^+), 389 (MNa^+); HRMS (ESI) calculated for $\text{C}_{18}\text{H}_{17}\text{F}_3\text{N}_2\text{O}_3$ (MNa^+) 389.1083, found 389.1082.

4.1.3.3. (*E*)-*N*-hydroxy-3-(2-oxo-1-(3-(4-(trifluoromethyl)phenyl)propyl)-1,2-dihydropyridin-3-yl)acrylamide (**4c**). Yellow solid (74 mg, 33.2%). MP: 47–49 °C; ^1H NMR (500 MHz, $\text{DMSO}-d_6$) δ 7.79–7.67 (m, 2H), 7.56 (dd, 4H, $J_A = 22.0$ Hz, 5.5 Hz), 7.45–7.32 (m, 1H), 7.11 (dd, 1H, $J_A = 15.0$ Hz, $J_B = 7.0$ Hz), 6.29 (dt, 1H, $J_A = 39.0$ Hz, $J_B = 7.0$ Hz), 3.98 (dt, 2H, $J_A = 26.0$ Hz, $J_B = 7.0$ Hz), 2.73 (t, 2H, $J = 7.5$ Hz), 2.09–1.98 (m, 2H); ESI (m/z) 367 (MH^+), 389 (MNa); HRMS (ESI) calcd for $\text{C}_{18}\text{H}_{17}\text{F}_3\text{N}_2\text{O}_3$ (MH^+) 367.1264, found 367.1266.

4.1.3.4. (*E*)-3-(1-(3-(2-chlorophenyl)propyl)-2-oxo-1,2-dihydropyridin-3-yl)-*N*-hydroxyacrylamide (**4d**). Orange oil (44 mg, 44.7%). ^1H NMR (500 MHz, $\text{DMSO}-d_6$) δ 10.76 (s, 1H), 8.92 (d, 1H, $J = 14.0$ Hz), 7.80–7.68 (m, 2H), 7.39–7.34 (m, 3H), 7.26–7.19 (m, 2H), 7.13 (d, 1H, $J = 15.5$ Hz), 6.32 (d, 1H, $J = 6.0$ Hz), 4.00 (dt, 2H, $J_A = 25.0$ Hz, $J_B = 6.5$ Hz), 2.70 (t, 2H, $J = 7.5$ Hz), 1.94 (d, 2H, $J = 6.5$ Hz); ESI (m/z) 333 (MH^+), 355 (MNa^+); HRMS (ESI) calculated for $\text{C}_{17}\text{H}_{17}\text{ClN}_2\text{O}_3$ (MH^+) 333.1000, found 333.0997.

4.1.3.5. (*E*)-3-(1-(3-(3-chlorophenyl)propyl)-2-oxo-1,2-dihydropyridin-3-yl)-*N*-hydroxyacrylamide (**4e**). Light brown solid (238.0 mg, 27.81%). MP: 137–139 °C; ^1H NMR (400 MHz, $\text{DMSO}-d_6$)

δ 10.74 (s, 1H), 8.94 (s, 1H), 7.77 (d, 1H, $J = 6.0$ Hz), 7.69 (d, 1H, $J = 6.8$ Hz), 7.37–7.29 (m, 3H), 7.25 (d, 1H, $J = 8.4$ Hz), 7.19 (d, 1H, $J = 7.6$ Hz), 7.12 (d, 1H, $J = 15.6$ Hz), 6.33 (t, 1H, $J = 6.8$ Hz), 3.98 (t, 2H, $J = 7.2$ Hz), 2.63 (t, 2H, $J = 7.6$ Hz), 2.01–1.94 (m, 2H); ESI (m/z) 333 (MH^+), 355 (MNa^+); HRMS (ESI) calculated for $C_{17}H_{17}ClN_2O_3$ (MH^+) 333.1000, found 333.0994.

4.1.3.6. (*E*)-3-(1-(3-(4-chlorophenyl)propyl)-2-oxo-1,2-dihydropyridin-3-yl)-*N*-hydroxyacrylamide (**4f**). Light brown solid (242.0 mg, 45.25%). MP: 140–143 °C; 1H NMR (400 MHz, DMSO- d_6) δ 10.75 (s, 1H), 8.95 (s, 1H), 7.78 (d, 1H, $J = 6.4$ Hz), 7.69 (d, 1H, $J = 6.8$ Hz), 7.37–7.24 (m, 5H), 7.12 (d, 1H, $J = 15.6$ Hz), 6.33 (t, 1H, $J = 6.6$ Hz), 3.97 (t, 2H, $J = 7.2$ Hz), 2.61 (t, 2H, $J = 7.6$ Hz), 1.99–1.92 (m, 2H); ^{13}C NMR (100 MHz, DMSO- d_6) δ 167.7, 160.4, 144.0, 142.4, 141.3, 133.3, 130.5, 128.5, 127.3, 126.3, 123.5, 118.8, 105.9, 51.7, 49.2, 32.1, 30.2; ESI (m/z) 334 (MH^+), 356 (MNa^+), 332 (MH^-).

4.1.3.7. (*E*)-*N*-hydroxy-3-(1-(3-(2-methoxyphenyl)propyl)-2-oxo-1,2-dihydropyridin-3-yl)acrylamide (**4g**). Orange solid (31.9 mg, 1.2%). MP: 150–152 °C; 1H NMR (500 MHz, DMSO- d_6) δ 10.75 (s, 1H), 8.94 (s, 1H), 7.79–7.69 (m, 2H), 7.34 (d, 1H, $J = 16.0$ Hz), 7.19–7.14 (m, 3H), 6.94 (d, 1H, $J = 7.5$ Hz), 6.86 (t, 2H, $J = 7.2$ Hz), 6.33 (t, 1H, $J = 6.8$ Hz), 3.98 (t, 2H, $J = 7.5$ Hz), 3.76 (s, 3H), 2.56 (t, 2H, $J = 7.8$ Hz), 1.91 (t, 2H, $J = 7.5$ Hz); ESI (m/z) 328 (MH^+), 351 (MNa^+); HRMS (ESI) calculated for $C_{18}H_{20}N_2O_4$ (MH^+) 329.1496, found 329.1494.

4.1.3.8. (*E*)-*N*-hydroxy-3-(1-(3-(naphthalen-1-yl)propyl)-2-oxo-1,2-dihydropyridin-3-yl)acrylamide (**4h**). Yellow solid (8.1 mg, 8.7%). MP: 182–184 °C; 1H NMR (500 MHz, DMSO- d_6) δ 10.74 (s, 1H), 8.94 (s, 1H), 8.01 (d, 1H), 7.93–7.91 (m, 1H), 7.87–7.85 (m, 1H), 7.78 (d, 1H, $J = 7.5$ Hz), 7.71 (d, 1H, $J = 7.5$ Hz), 7.55–7.50 (m, 2H), 7.44–7.38 (m, 2H), 7.35 (d, 1H, $J = 15.5$ Hz), 7.13 (d, 1H, $J = 15.5$ Hz), 6.35 (t, 1H, $J = 6.8$ Hz), 4.11 (t, 2H, $J = 7.2$ Hz), 3.08 (t, 2H, $J = 7.8$ Hz), 2.07 (t, 2H, $J = 7.2$ Hz); ESI (m/z) 349 (MH^+), 371 (MNa^+); HRMS (ESI) calculated for $C_{21}H_{20}N_2O_3$ (MH^+) 349.1547, found 349.1542.

4.1.3.9. (*E*)-*N*-hydroxy-3-(2-oxo-1-(3-(2-(trifluoromethoxy)phenyl)propyl)-1,2-dihydropyridin-3-yl)acrylamide (**4i**). Light brown solid (220 mg, 73.8%). MP: 91–93 °C; 1H NMR (400 MHz, DMSO- d_6) δ 10.75 (s, 1H), 8.94 (s, 1H), 7.78 (d, 1H, $J = 6.0$ Hz), 7.69 (d, 1H, $J = 6.4$ Hz), 7.36–7.25 (m, 5H), 7.12 (d, 1H, $J = 15.6$ Hz), 6.33 (t, 1H, $J = 6.6$ Hz), 3.99 (t, 2H, $J = 7.0$ Hz), 2.65 (t, 2H, $J = 7.6$ Hz), 2.02–1.94 (m, 2H); ESI (m/z) 383 (MH^+), 405 (MNa^+), 381 (MH^-); HRMS (ESI) calculated for $C_{18}H_{17}F_3N_2O_4$ (MNa^+) 405.1033, found 405.1030.

4.1.3.10. (*E*)-*N*-hydroxy-3-(2-oxo-1-(3-(3-(trifluoromethoxy)phenyl)propyl)-1,2-dihydropyridin-3-yl)acrylamide (**4j**). Light brown solid (17.0 mg, 5.7%). 1H NMR (400 MHz, DMSO- d_6) δ 10.75 (s, 1H), 8.94 (s, 1H), 7.78 (d, 1H, $J = 6.0$ Hz), 7.69 (d, 1H, $J = 6.4$ Hz), 7.36–7.25 (m, 5H), 7.12 (d, 1H, $J = 15.6$ Hz), 6.33 (t, 1H, $J = 6.6$ Hz), 3.99 (t, 2H, $J = 7.0$ Hz), 2.65 (t, 2H, $J = 7.6$ Hz), 2.02–1.94 (m, 2H); ESI (m/z) 383 (MH^+), 405 (MNa^+), 381 (MH^-); HRMS (ESI) calculated for $C_{18}H_{17}F_3N_2O_4$ (MNa^+) 405.1033, found 405.1035.

4.1.3.11. (*E*)-*N*-hydroxy-3-(2-oxo-1-(3-(4-(trifluoromethoxy)phenyl)propyl)-1,2-dihydropyridin-3-yl)acrylamide (**4k**). Orange oil (220 mg, 73.8%). 1H NMR (500 MHz, DMSO- d_6) δ 10.75 (s, 1H), 8.92 (d, 1H, $J = 15.5$ Hz), 7.78 (d, 1H, $J = 6.5$ Hz), 7.71 (t, 1H, $J = 7.0$ Hz), 7.34 (dd, 3H, $J_A = 5.5$ Hz, $J_B = 9.0$ Hz), 7.27 (d, 2H, $J = 8.0$ Hz), 6.33 (t, 1H, $J = 7.0$ Hz), 3.98 (dt, 2H, $J_A = 25.0$ Hz, $J_B = 7.5$ Hz), 2.68–2.64 (m, 2H), 2.10 (s, 1H), 2.02–1.94 (m, 2H); ESI (m/z) 383 (MH^+), 405 (MNa^+).

4.1.3.12. (*E*)-*N*-hydroxy-3-(2-oxo-1-((*E*)-3-(3-(trifluoromethyl)phenyl)allyl)-1,2-dihydropyridin-3-yl)acrylamide (**7a**). Pale gray solid (150 mg, 62.0%). MP: 169–172 °C; 1H NMR (500 MHz, DMSO- d_6) δ 10.75 (s, 1H), 8.93 (s, 1H), 7.80 (d, 2H, $J = 11.0$ Hz), 7.75 (t, 2H, $J = 8.5$ Hz), 7.60 (d, 1H, $J = 7.5$ Hz), 7.56 (d, 1H, $J = 8.5$ Hz), 7.37 (d, 1H, $J = 15.5$ Hz), 7.13 (d, 1H, $J = 15.5$ Hz), 6.67–6.57 (m, 2H), 6.38 (t, 1H, $J = 7.0$ Hz), 4.78 (d, 2H, $J = 5.5$ Hz); ESI (m/z) 365 (MH^+), 387 (MNa^+); HRMS (ESI) calculated for $C_{18}H_{15}F_3N_2O_3$ (MH^+) 365.1108, found 365.1103.

4.1.3.13. (*E*)-3-(1-((*E*)-3-(2-bromophenyl)allyl)-2-oxo-1,2-dihydropyridin-3-yl)-*N*-hydroxyacrylamide (**7b**). Orange solid (100 mg, 52.5%). 1H NMR (500 MHz, DMSO- d_6) δ 10.76 (s, 1H), 7.84 (d, 1H, $J = 6.5$ Hz), 7.75 (d, 1H, $J = 7.0$ Hz), 7.68 (d, 1H, $J = 8.0$ Hz), 7.61 (dt, 1H, $J_A = 8.0$ Hz, $J_B = 1.0$ Hz), 7.38–7.33 (m, 2H), 7.22–7.19 (m, 1H), 7.14 (d, 1H, $J = 15.5$ Hz), 6.78 (d, 1H, $J = 15.5$ Hz), 6.48–6.41 (m, 1H), 6.38 (t, 1H, $J = 6.0$ Hz), 4.81 (d, 2H, $J = 6.0$ Hz); ESI (m/z) 375 (MH^+), 399 (MNa^+); HRMS (ESI) calculated for $C_{17}H_{15}BrN_2O_3$ (MH^+) 375.0339, found 375.0329.

4.1.3.14. (*E*)-3-(1-((*E*)-3-(3-bromophenyl)allyl)-2-oxo-1,2-dihydropyridin-3-yl)-*N*-hydroxyacrylamide (**7c**). Orange solid (100 mg, 51.5%). MP: 159–162 °C; 1H NMR (500 MHz, DMSO- d_6) δ 10.76 (s, 1H), 8.94 (s, 1H), 7.80 (dd, 1H, $J_A = 5.0$ Hz, $J_B = 2.0$ Hz), 7.73 (dd, 1H, $J_A = 5.5$ Hz, $J_B = 1.5$ Hz), 7.67 (s, 1H), 7.45–7.43 (m, 2H), 7.37 (d, 1H, $J = 15.5$ Hz), 7.28 (t, 1H, $J = 8.0$ Hz), 7.13 (d, 1H, $J = 15.5$ Hz), 6.52–6.50 (m, 2H), 6.38 (t, 1H, $J = 7.0$ Hz), 4.75 (d, 2H, $J = 5.0$ Hz); ESI (m/z) 375 (MH^+), 399 (MNa^+); HRMS (ESI) calculated for $C_{17}H_{15}BrN_2O_3$ (MH^+) 375.0339, found 375.0334.

4.1.3.15. (*E*)-3-(1-((*E*)-3-(4-bromophenyl)allyl)-2-oxo-1,2-dihydropyridin-3-yl)-*N*-hydroxyacrylamide (**7d**). Orange solid (70 mg, 29.7%). MP: 108–111 °C; 1H NMR (500 MHz, DMSO- d_6) δ 10.76 (s, 1H), 8.94 (s, 1H), 7.81 (dd, 1H, $J_A = 5.0$ Hz, $J_B = 2.0$ Hz), 7.73 (d, 1H, $J = 7.0$ Hz), 7.51 (d, 2H, $J = 8.5$ Hz), 7.40 (d, 2H, $J = 8.5$ Hz), 7.19 (dd, 1H, $J_A = 6.0$ Hz, $J_B = 2.5$ Hz), 6.55 (d, 1H, $J = 16.0$ Hz), 6.38 (t, 1H, $J = 6.5$ Hz), 4.73 (d, 2H, $J = 6.0$ Hz); ESI (m/z) 375 (MH^+), 399 (MNa^+); HRMS (ESI) calculated for $C_{17}H_{15}BrN_2O_3$ (MH^+) 375.0339, found 375.0335.

4.1.3.16. (*E*)-3-(1-((*E*)-3-(3-chlorophenyl)allyl)-2-oxo-1,2-dihydropyridin-3-yl)-*N*-hydroxyacrylamide (**7e**). Pale gray solid (190 mg, 47.4%). MP: 150–155 °C; 1H NMR (500 MHz, DMSO- d_6) δ 10.75 (s, 1H), 8.94 (s, 1H), 7.81–7.79 (m, 1H), 7.73 (d, 1H, $J = 7.0$ Hz), 7.53 (s, 1H), 7.40–7.29 (m, 4H), 7.13 (d, 1H, $J = 15.5$ Hz), 6.57–6.48 (m, 2H), 6.38 (t, 1H, $J = 6.5$ Hz), 4.75 (d, 2H, $J = 5.0$ Hz); ESI (m/z) 331 (MH^+), 353 (MNa^+); HRMS (ESI) calculated for $C_{17}H_{15}ClN_2O_3$ (MH^+) 331.0844, found 331.0839.

4.1.3.17. (*E*)-*N*-hydroxy-3-(1-((*E*)-3-(3-methoxyphenyl)allyl)-2-oxo-1,2-dihydropyridin-3-yl)acrylamide (**7f**). Pale yellow solid (140 mg, 37.6%). 1H NMR (500 MHz, DMSO- d_6) δ 10.74–10.73 (m, 1H), 8.91 (s, 1H), 7.80 (dd, 1H, $J_A = 4.5$ Hz, $J_B = 2.0$ Hz), 7.72 (dd, 1H, $J_A = 5.0$ Hz, $J_B = 2.0$ Hz), 7.36 (d, 1H, $J = 15.5$ Hz), 7.25–7.21 (m, 1H), 7.15–7.12 (m, 1H), 6.99–6.98 (m, 2H), 6.86–6.80 (m, 1H), 6.54 (d, 1H, $J = 16.0$ Hz), 6.44–6.36 (m, 2H), 4.74 (d, 2H, $J = 5.5$ Hz), 3.74 (s, 3H); ESI (m/z) 327 (MH^+), 349 (MNa^+); HRMS (ESI) calculated for $C_{18}H_{18}N_2O_4$ (MH^+) 327.1339, found 327.1336.

4.1.3.18. (*E*)-*N*-hydroxy-3-(2-oxo-1-((*E*)-3-(3-(trifluoromethoxy)phenyl)allyl)-1,2-dihydropyridin-3-yl)acrylamide (**7g**). Pale yellow solid (240 mg, 53.1%). MP: 159–162 °C; 1H NMR (500 MHz, DMSO- d_6) δ 10.74 (s, 1H), 8.92 (s, 1H), 7.80 (dd, 1H, $J_A = 4.5$ Hz, $J_B = 1.5$ Hz), 7.73 (d, 1H, $J = 5.5$ Hz), 7.48–7.43 (m, 3H), 7.36 (d, 1H, $J = 15.5$ Hz), 7.24 (d, 1H, $J = 7.5$ Hz), 7.12 (d, 1H, $J = 15.5$ Hz), 6.61–6.51 (m, 2H),

6.37 (t, 1H, $J = 7.0$ Hz), 4.76 (d, 2H, $J = 5.0$ Hz); ESI (m/z) 381 (MH⁺), 403 (MNa⁺); HRMS (ESI) calculated for C₁₈H₁₅F₃N₂O₄ (MH⁺) 381.1057, found 381.1052.

4.1.3.19. (*E*)-*N*-hydroxy-3-(1-((*E*)-3-(naphthalen-1-yl)allyl)-2-oxo-1,2-dihydropyridin-3-yl)acrylamide (**7h**). Pale yellow solid (10 mg, 12.2%). MP: 146–149 °C; ¹H NMR (500 MHz, DMSO-*d*₆) δ 10.77 (s, 1H), 8.93 (s, 1H), 8.14 (d, 1H, $J = 8.5$ Hz), 7.94–7.92 (m, 2H), 7.87 (d, 1H, $J = 8.5$ Hz), 7.76–7.74 (m, 1H), 7.67 (d, 1H, $J = 7.0$ Hz), 7.58–7.52 (m, 2H), 7.47 (dd, 2H, $J_A = 20.5$ Hz, $J_B = 7.5$ Hz), 7.38 (d, 1H, $J = 15.5$ Hz), 7.16 (d, 1H, $J = 15.5$ Hz), 6.43 (dt, 2H, $J_A = 17.0$ Hz, $J_B = 6.0$ Hz), 4.88 (d, 2H, $J = 6.0$ Hz); ESI (m/z) 347 (MH⁺), 369 (MNa⁺); HRMS (ESI) calcd for C₂₁H₁₈N₂O₃ (MH⁺) 347.1390, found 347.1390.

4.1.3.20. (*E*)-*N*-hydroxy-3-(1-((*E*)-3-(naphthalen-2-yl)allyl)-2-oxo-1,2-dihydropyridin-3-yl)acrylamide (**7i**). Pale orange solid (30 mg, 33.3%). MP: 199–202 °C; ¹H NMR (500 MHz, DMSO-*d*₆) δ 10.74 (s, 1H), 3.91 (s, 1H), 7.88–7.85 (m, 5H), 7.75–7.73 (m, 1H), 7.68 (dd, 1H, $J_A = 7.5$ Hz, $J_B = 1.5$ Hz), 7.50–7.45 (m, 2H), 7.37 (d, 1H, $J = 15.5$ Hz), 7.15 (d, 1H, $J = 15.5$ Hz), 6.72 (d, 1H, $J = 16.0$ Hz), 6.59–6.53 (m, 1H), 6.39 (t, 1H, $J = 7.0$ Hz), 4.81 (d, 2H, $J = 5.5$ Hz). ¹³C NMR (125 MHz, DMSO-*d*₆) δ 164.0, 160.4, 141.66, 139.8, 135.4, 133.9, 133.5, 133.1, 133.0, 128.6, 128.3, 128.0, 126.8, 126.7, 126.53, 125.6, 124.7123.9, 121.1, 106.2, 50.8; ESI (m/z) 346 (MH⁺), 368 (MNa⁺); HRMS (ESI) calcd for C₂₁H₁₈N₂O₃ (MNa⁺) 369.1210, found 369.1207.

4.1.3.21. (*E*)-*N*-hydroxy-3-(2-oxo-1-((*E*)-3-(quinolin-2-yl)allyl)-1,2-dihydropyridin-3-yl)acrylamide (**7j**). Brown solid (72 mg, 48.1%). ¹H NMR (400 MHz, DMSO-*d*₆) δ 10.73 (s, 1H), 8.91 (s, 1H), 8.28 (d, 1H, $J = 8.4$ Hz), 7.89 (d, 2H, $J = 8.0$ Hz), 7.84 (d, 1H, $J = 6.0$ Hz), 7.75–7.67 (m, 3H), 7.51 (t, 1H, $J = 7.4$ Hz), 7.35 (d, 1H, $J = 16.0$ Hz), 7.12 (d, 1H, $J = 15.6$ Hz), 7.02–6.95 (m, 1H), 6.64 (d, 1H, $J = 16.0$ Hz), 6.38 (t, 1H, $J = 6.8$ Hz), 4.84 (d, 2H, $J = 5.2$ Hz); ESI (m/z) 347 (MH⁺), 349 (MNa⁺); HRMS (ESI) calcd for C₂₀H₁₇N₃O₃ (MNa⁺) 370.1162, found 370.1161.

4.1.3.22. (*E*)-3-(1-cinnamyl-2-oxo-1,2-dihydropyridin-3-yl)-*N*-hydroxyacrylamide (**7k**). Orange solid (200 mg, 44.0%). MP: 144–147 °C; ¹H NMR (500 MHz, DMSO-*d*₆) δ 7.73 (t, 1H, $J = 6.5$ Hz), 7.42–7.13 (m, 6H), 6.57 (dd, 1H, $J_A = 12.5$ Hz, $J_B = 3.5$ Hz), 6.42–6.35 (m, 2H), 4.72 (dd, 2H, $J_A = 17.5$ Hz, $J_B = 6.0$ Hz); ¹³C NMR (125 MHz, DMSO-*d*₆) δ 164.0, 160.4, 141.6, 139.7, 136.3, 135.4, 133.3, 129.08(2), 126.32, 126.81(2), 124.9, 124.7, 121.1, 106.2, 50.8; ESI (m/z) 297 (MH⁺), 319 (MNa⁺); HRMS (ESI) calcd for C₁₇H₁₆N₂O₃ (MH⁺) 297.1234, found 297.1232.

4.2. Biological assays

4.2.1. HDAC inhibition

4.2.1.1. HDAC inhibitory assays. The IC₅₀ values of HDAC inhibitors were determined using the HDAC fluorometric assay/drug discovery kit (BioMol, now ENZO Life Sciences, Plymouth Meeting, PA, USA) which is based on the unique Fluor de Lys system (fluorogenic histone deacetylase lysyl substrate/developer). It is designed to measure histone deacetylase (HDAC) activity. In this assay, we used nuclear extracts from the human cervical cancer cell line HeLa (from 6 to 9 mg protein/mL⁻¹ in 0.1 M KCl, 20 mM HEPES/NaOH, pH 7.9, 20% (v/v) glycerol, 0.2 mM EDTA, 0.5 mM DTT, 0.5 mM PMSF) [26]. The HeLa cell nuclear extract contained all class I HDACs (HDAC1, HDAC2, HDAC3, and HDAC8), class II HDACs (HDAC4–7, 9, and 10), and human homolog of yeast Sir2, SIRT1. SAHA was used as the positive control. A nuclear fraction of HeLa cells (15 μL of 30 ×) was diluted to 10 μL with the assay buffer containing the HDAC inhibitors and the Fluor de Lys substrate (lysine with an acetylated

amino group on the side chain) at a final concentration of 100 μM. The samples were incubated for 30 min at 37 °C and then added to the Fluor de Lys developer (25 μL) for 10 min at rt). The samples were measured using a microtiter-plate-reading fluorimeter capable of excitation at a wavelength at 360 nm and detection of emitted light at 460 nm.

4.2.2. RUNX3 transcriptional activation

The percentage of RUNX transcriptional activation relative to FGF-2 was determined by using the C2C12-6xOSE cell line with the luciferase assay system. The C2C12-6xOSE cell line was kindly provided by Prof. Hyun-Mo Ryoo (Seoul National University, Seoul, South Korea). Cells were plated at 1 × 10⁴ cells per well in 96-well plates. Fibroblast growth factor (FGF)-2 and drugs (1 μM each) were added to cells the next day. After 24 h, cells were harvested and analyzed by luciferase assay with the Bright-Glo luciferase assay system according to the manufacturer's protocol (Promega, Madison, WI, USA). Lysates were analyzed with the GloMax-Multi Detection System (Promega). FGF-2 was used as a positive control for RUNX activation.

4.2.3. Cancer cell growth inhibitory assays

The final concentrations of reagent used to treat cells were 0.1, 0.3, 1, 3, and 10 μg/mL. Cells were harvested from exponential phase cultures by trypsinization, counted, and plated into 96-well plates. Optimal seeding densities for various human tumor cell lines (HCT-15, PC-3, NUGC-3, ACHN, MDA-MB-231, and NCI-H23) were determined to ensure exponential growth during a 5-day assay. The sulforhodamine B assay was performed with minor modifications [27]. The culture medium was aspirated prior to fixation of the cells by the addition of 50 μL of 50% cold trichloroacetic acid. After 1 h incubation at 4 °C, cells were washed five times with deionized water. After 24 h, the cells were stained with 100 μL of 1 × sulforhodamine B (SRB, Sigma-Aldrich, St. Louis, MO, USA) dissolved in 1% acetic acid for at least 30 min and subsequently washed four times with 1% acetic acid to remove unbound stain. The plates were left to dry at room temperature for 24 h; subsequently, bound protein stain was solubilized with 100 μL of 10 mM unbuffered Tris and the optical density (OD) was read at 540 nm.

4.2.4. Liver microsomal stability assay

Microsomal incubations were conducted in triplicate in 0.1 M potassium phosphate buffer (pH 7.4) in eight-well tube strips. To study NADPH-dependent metabolic stability, test compounds (1 mM) were incubated with pooled mouse liver microsomes at a final concentration of 0.5 mgmL⁻¹ (BD Genetex, USA), in the presence of NADPH (Sigma-Aldrich, St. Louis, MO, USA) in a final volume of 160 μL. Buspirone was used as a positive control. The test compounds and microsomes were pre-incubated at 37 °C for 5 min, and the reaction was initiated by adding NADPH. The reaction was terminated at 0 min and 30 min by the addition of 160 μL of ice-cold CH₃CN. The values for % remaining were analyzed by a liquid chromatography electrospray ionization tandem mass spectrometry (LC-ESI-MS/MS) for quantitation of compounds. These experiments were performed at the KRIBB Bio-Evaluation Center (Chungbuk, Korea).

4.2.5. Western blot analysis

4.2.5.1. Western blot analysis. After cells were lysed with radioimmuno-precipitation assay (RIPA) buffer (25 mM Tris-HCl, pH 7.6, 150 mM NaCl, 1% NP-40, 1% sodium deoxycholate, 0.1% sodium dodecyl sulfate, SDS), protein concentrations were determined with a bicinchoninic acid assay (BCA) protein assay kit (Pierce, Rockford, IL, USA). Equal amounts of protein were fractionated by SDS-polyacrylamide gel electrophoresis (PAGE) and

transferred onto a nitrocellulose membrane (BioRad, Richmond, CA, USA). After blocking with 5% skim milk in phosphate-buffered saline (PBS) containing 0.1% Tween 20, membranes were incubated with the appropriate primary antibodies at 4 °C overnight. Proteins were detected with horseradish peroxidase (HRP) conjugated secondary antibodies and an enhanced chemiluminescence (ECL) kit (Amer-sham Pharmacia Biotech, Buckinghamshire, U.K.). Antibodies against myc (9E10) and tubulin were from Santa Cruz Biotechnology (Santa Cruz, CA, USA). Acetylated lysine antibody was purchased from Cell Signaling (Danvers, MA, USA).

4.2.5.2. Immunoprecipitation analysis. The myc-RUNX3 expression vector was kindly provided by Prof. Suk-Chul Bae (Chungbuk National University, Cheongju, South Korea). The myc-RUNX3 expression vector was transfected into HEK293 cells with Lipofect-amine 2000 (Invitrogen). Transfected cells were treated with HDAC inhibitors at 1 μM the next day for an additional 24 h. Cells were lysed in ice-cold lysis buffer (25 mM HEPES, pH 7.5, 150 mM NaCl, 1% Nonidet P-40, 0.25% sodium deoxycholate, 10% glycerol, 25 mM NaF, 1 mM EDTA, 1 mM Na₃VO₄) and cleared by centrifugation. For immunoprecipitation experiments, 500 mg of protein was incubated with anti-myc antibody and precipitated with protein G beads (Pierce) at 4 °C. The beads were washed three times with cold lysis buffer, and the immunoprecipitates were analyzed by Western blot with an antibody against acetylated lysine.

4.2.6. In vivo xenograft studies

Six-week-old female specified-pathogen-free (SPF) BALB/c nude mice were purchased from Charles River Laboratories (Yokohama, Japan) and maintained in accordance with the Animal Research Committee's Guidelines at the Korea Research Institute of Bioscience and Biotechnology (KRIBB). MKN28 cells (4×10^7 /animal) were injected subcutaneously into the flank area. When tumors reached a volume of 50–80 mm³, as measured with a digital caliper, mice were randomized into groups of four animals each to receive either vehicle control, **7c**, **7j**, or **7k**. The drugs were orally administered at 30 mg/kg in 10% DMAC and 10% Tween80 (Sigma) in saline daily for 2 weeks. Tumor growth was measured three times a week until the end of the study. The length and width of the tumor were measured with calipers. Tumor volume was calculated according to the formula for an ellipse, volume = $0.523 \times (\text{long dimension}) \times (\text{short dimension})^2$.

4.2.7. In vivo pharmacokinetic studies

Animal studies were approved by the Institutional Animal Care and Use Committee at KRIBB and conducted as described previously with minor modifications [28]. Briefly, male ICR mice (5–6 weeks old, body weight 25–30 g), purchased from Koatech Co. (Kyeonggi, Republic of Korea), were given a single dose of **7k** intravenously (iv, 2 mg/kg, n = 3) or orally (po, 10 mg/kg, n = 3). Dosing solutions were prepared in dimethylacetamide (DMAC)/20% 2-hydroxypropyl-β-cyclodextrin (10/90, v/v %) for iv administration, and DMAC/vitamin E TPGS 80/25% Solutol HS 15 (10/10/80, v/v %) for po administration, and administered at dosing volumes of 5 and 10 mL/kg for iv and po, respectively. A 100 μL aliquot of each plasma sample was prepared, and three volumes of ice-cold acetonitrile containing carbamazepine (internal standard) were added. The mixture was centrifuged at 910g for 10 min, and the supernatant was subjected to LC–MS/MS analysis. Pharmacokinetic parameters were calculated by standard noncompartmental analysis of plasma concentration–time profiles using Kinetic 4.4.1 (Thermo Fisher Scientific, Inc., Woburn, MA, USA). The areas under the plasma concentration–time curves (AUC) were calculated by the linear–trapezoidal method. Systemic plasma clearance (CL_p)

was calculated as follows: $CL_p = \text{dose}/AUC_{inf}$. Terminal elimination half-life ($t_{1/2}$) was calculated by the following equation: $t_{1/2} = 0.693/\lambda_z$ where λ_z is the terminal disposition rate constant. Volume of distribution at steady state (V_{ss}) was calculated as follows: $V_{ss} = \text{dose} \times AUMC_{inf}/(AUC_{inf})^2$, where AUMC_{inf} is the area under the first moment of the plasma concentration–time curve extrapolated to infinity. Oral bioavailability (F) was calculated as follows: $F(\%) = (AUC_{po}/AUC_{iv}) \times (\text{dose}_{iv}/\text{dose}_{po}) \times 100$.

4.3. In silico studies

Molecular docking studies were performed using the docking software LigandFit and Calculate Binding Energies within the software package Discovery Studio 2017 (Accelrys, San Diego, CA, USA). The crystal structure of human HDAC2 (PDB code: 3MAX) obtained from the Protein Data Bank was refined to remove water molecules and add hydrogen atoms to the entire enzyme at pH 7.4. A binding pocket of the native ligand (SAHA) was selected as the binding site for the study. The consistent force field (CFF) function was selected as the energy grid, and the Monte Carlo trial method was used to roughly search the conformations when pyridone-based HDAC inhibitors were docked into the HDAC enzyme. The ligands were then optimized using the CHARMM force field function.

Acknowledgement

This research was supported by a grant from the Translational Research Center for Protein Function Control (TRCP 2016R1A5A1004694), the Ministry of Science, ICT and Future Planning (Grant NRF-2013M3A6A4072536), the Basic Science Research Program through the National Research Foundation of Korea funded by the Ministry of Education (Grant NRF-2015R1A6A3A01020077), the Korea Health Technology R&D Project through the Korea Health Industry Development Institute (KHIDI), funded by the Ministry of Health & Welfare, Republic of Korea (HI14C1324), the Yonsei University Research Fund (Post Doc. Researcher Supporting Program 2015-12-0005), and the KRIBB Research Initiative Program.

Appendix A. Supplementary data

Supplementary data related to this article can be found at <http://dx.doi.org/10.1016/j.ejmech.2016.11.055>.

Myc-tagged RUNX3 (Myc-RUNX3) was expressed in HEK293 cells. Acetylated RUNX3 levels were analyzed by immunoprecipitation in HEK293 cells following treatment with 1 μM indicated test compound. (A) the Western blot of alkyl linker derivatives; (B) the Western blot of olefin linker derivatives; (C) relative expression of RUNX3 acetylation based on the results of the Western blot.

30 mg/kg, q1d × 14 on the growth of a MKN28 human stomach tumor xenograft in nude mice; (A) Average body weight changes; (B) average tumor volume; (C) average tumor weight in mice treated with vehicle control (V.C.).

References

- [1] S.L. Berger, T. Kouzarides, R. Shiekhattar, A. Shilatifard, An operational definition of epigenetics, *Genes & Dev.* 23 (2009) 781–783.
- [2] M. Esteller, Epigenetics in cancer, *N. Engl. J. Med.* 358 (2008) 1148–1159.
- [3] P.A. Jones, S.B. Baylin, The epigenomics of cancer, *Cell* 128 (2007) 683–692.
- [4] M. Rodriguez-Paredes, M. Esteller, Cancer epigenetics reaches mainstream oncology, *Nat. Med.* 17 (2011) 330–339.
- [5] N. Sengupta, E. Seto, Regulation of histone deacetylase activities, *J. Cell. Biochem.* 93 (2004) 57–67.
- [6] M. Dokmanovic, C. Clarke, P.A. Marks, Histone deacetylase inhibitors:

- overview and perspectives, *Mol. cancer Res. MCR* 5 (2007) 981–989.
- [7] J.E. Bolden, M.J. Peart, R.W. Johnstone, Anticancer activities of histone deacetylase inhibitors, *Nat. Rev. Drug Discov.* 5 (2006) 769–784.
- [8] M. Yoshida, [Potent and specific inhibition of mammalian histone deacetylase both in vivo and in vitro by trichostatin A], *Tanpakushitsu kakusan koso, Protein, nucleic acid. enzyme* 52 (2007) 1788–1789.
- [9] P.A. Marks, R. Breslow, Dimethyl sulfoxide to vorinostat: development of this histone deacetylase inhibitor as an anticancer drug, *Nat. Biotechnol.* 25 (2007) 84–90.
- [10] S. Belvedere, D.J. Witter, J. Yan, J.P. Secrist, V. Richon, T.A. Miller, Aminobisoxalyl hydroxamic acids (ASHAs): a potent new class of HDAC inhibitors, *Bioorg. Med. Chem. Lett.* 17 (2007) 3969–3971.
- [11] R.H. Wilting, J.H. Dannenberg, Epigenetic mechanisms in tumorigenesis, tumor cell heterogeneity and drug resistance, *Drug Resist. Updat. Rev. Comment. Antimicrob. anticancer Chemother.* 15 (2012) 21–38.
- [12] R. Popovic, J.D. Licht, Emerging epigenetic targets and therapies in cancer medicine, *Cancer Discov.* 2 (2012) 405–413.
- [13] C.H. Arrowsmith, C. Bountra, P.V. Fish, K. Lee, M. Schapira, Epigenetic protein families: a new frontier for drug discovery, *Nat. Rev. Drug Discov.* 11 (2012) 384–400.
- [14] R. Holliday, G.W. Grigg, DNA methylation and mutation, *Mutat. Res.* 285 (1993) 61–67.
- [15] Q.L. Li, K. Ito, C. Sakakura, H. Fukamachi, K. Inoue, X.Z. Chi, K.Y. Lee, S. Nomura, C.W. Lee, S.B. Han, H.M. Kim, W.J. Kim, H. Yamamoto, N. Yamashita, T. Yano, T. Ikeda, S. Itohara, J. Inazawa, T. Abe, A. Hagiwara, H. Yamagishi, A. Ooe, A. Kaneda, T. Sugimura, T. Ushijima, S.C. Bae, Y. Ito, Causal relationship between the loss of RUNX3 expression and gastric cancer, *Cell* 109 (2002) 113–124.
- [16] X.Z. Chi, J.O. Yang, K.Y. Lee, K. Ito, C. Sakakura, Q.L. Li, H.R. Kim, E.J. Cha, Y.H. Lee, A. Kaneda, T. Ushijima, W.J. Kim, Y. Ito, S.C. Bae, RUNX3 suppresses gastric epithelial cell growth by inducing p21(WAF1/Cip1) expression in cooperation with transforming growth factor (beta)-activated SMAD, *Mol. Cell. Biol.* 25 (2005) 8097–8107.
- [17] S.C. Bae, J.K. Choi, Tumor suppressor activity of RUNX3, *Oncogene* 23 (2004) 4336–4340.
- [18] Y.M. Lee, Control of RUNX3 by histone methyltransferases, *J. Cell. Biochem.* 112 (2011) 394–400.
- [19] Y.H. Jin, E.J. Jeon, Q.L. Li, Y.H. Lee, J.K. Choi, W.J. Kim, K.Y. Lee, S.C. Bae, Transforming growth factor-beta stimulates p300-dependent RUNX3 acetylation, which inhibits ubiquitination-mediated degradation, *J. Biol. Chem.* 279 (2004) 29409–29417.
- [20] H.J. Kim, S.C. Bae, Histone deacetylase inhibitors: molecular mechanisms of action and clinical trials as anti-cancer drugs, *Am. J. Transl. Res.* 3 (2011) 166–179.
- [21] M. Cho, E. Choi, J.H. Kim, H. Kim, H.M. Kim, J.I. Lee, K.C. Hwang, H.J. Kim, G. Han, Lactam-based HDAC inhibitors for anticancer chemotherapy: restoration of RUNX3 by posttranslational modification and epigenetic control, *ChemMedChem* 9 (2014) 649–656.
- [22] M. Cho, E. Choi, J.S. Yang, C. Lee, J.J. Seo, B.S. Kim, S.J. Oh, H.M. Kim, K. Lee, S.K. Park, H.J. Kwon, G. Han, Discovery of pyridone-based histone deacetylase inhibitors: approaches for metabolic stability, *ChemMedChem* 8 (2013) 272–279.
- [23] H.M. Kim, D.K. Ryu, Y. Choi, B.W. Park, K. Lee, S.B. Han, C.W. Lee, M.R. Kang, J.S. Kang, S.K. Boovanahalli, S.K. Park, J.W. Han, T.G. Chun, H.Y. Lee, K.Y. Nam, E.H. Choi, G. Han, Structure-activity relationship studies of a series of novel delta-lactam-based histone deacetylase inhibitors, *J. Med. Chem.* 50 (2007) 2737–2741.
- [24] H.J. Kim, H.D. Park, J.H. Kim, J.Y. Cho, J.Y. Choi, J.K. Kim, H.J. Kim, H.I. Shin, H.M. Ryoo, Establishment and characterization of a stable cell line to evaluate cellular Runx2 activity, *J. Cell. Biochem.* 91 (2004) 1239–1247.
- [25] Q.L. Li, H.R. Kim, W.J. Kim, J.K. Choi, Y.H. Lee, H.M. Kim, L.S. Li, H. Kim, J. Chang, Y. Ito, K. Youl Lee, S.C. Bae, Transcriptional silencing of the RUNX3 gene by CpG hypermethylation is associated with lung cancer, *Biochem. biophysical Res. Commun.* 314 (2004) 223–228.
- [26] J.D. Dignam, R.M. Lebovitz, R.G. Roeder, Accurate transcription initiation by RNA polymerase II in a soluble extract from isolated mammalian nuclei, *Nucleic acids Res.* 11 (1983) 1475–1489.
- [27] P. Skehan, R. Storeng, D. Scudiero, A. Monks, J. McMahon, D. Vistica, J.T. Warren, H. Bokesch, S. Kenney, M.R. Boyd, New colorimetric cytotoxicity assay for anticancer-drug screening, *J. Natl. Cancer Inst.* 82 (1990) 1107–1112.
- [28] K. Lee, B.M. Kwon, K. Kim, J. Ryu, S.J. Oh, K.S. Lee, M.G. Kwon, S.K. Park, J.S. Kang, C.W. Lee, H.M. Kim, Plasma pharmacokinetics and metabolism of the antitumor drug candidate 2'-benzoyloxycinnamaldehyde in rats, *Xenobiotica; fate foreign Compd. Biol. Syst.* 39 (2009) 255–265.
- [29] E. Choi, C. Lee, M. Cho, J.J. Seo, J.S. Yang, S.J. Oh, K. Lee, S.K. Park, H.M. Kim, H.J. Kwon, G. Han, Property-based optimization of hydroxamate-based gamma-lactam HDAC inhibitors to improve their metabolic stability and pharmacokinetic profiles, *J. Med. Chem.* 55 (2012) 10766–10770.
- [30] J.S. Yang, C. Lee, M. Cho, H. Kim, J.H. Kian, S. Choi, S.J. Oh, J.S. Kang, J.H. Jeong, H.J. Kim, G. Han, Discovery of orally available runt-related transcription factor 3 (RUNX3) modulators for anticancer chemotherapy by epigenetic activation and protein stabilization, *J. Med. Chem.* 58 (2015) 3512–3521.